

JGR Planets

RESEARCH ARTICLE

10.1029/2024JE008540

Key Points:

- A 3-D General Circulation Model simulates the middle and upper atmospheric effects of energy balance and dynamics for a Venus-type exoplanet orbiting GJ 436
- Energy balance sensitivity shows 2×–4× Near InfraRed heating significantly alters dynamics and temperature across all modeled pressure levels
- CO₂ 15-μm cooling limits thermal escape, stabilizes dense CO₂-rich atmospheres, and shapes emission spectra on M-dwarf exo-Venus planets

Correspondence to:

C. D. Parkinson,
cparkinson@spacescience.org

Citation:

Parkinson, C. D., Bougner, S. W., Mills, F. P., Yung, Y. L., Brecht, A., Li, J., et al. (2025). Venus as an exoplanet: I. An initial exploration of the 3-D energy balance for a CO₂-rich exoplanetary atmosphere around the M-dwarf Star GJ 436. *Journal of Geophysical Research: Planets*, 130, e2024JE008540. <https://doi.org/10.1029/2024JE008540>

Received 11 NOV 2024

Accepted 14 SEP 2025

Venus as an Exoplanet: I. An Initial Exploration of the 3-D Energy Balance for a CO₂-Rich Exoplanetary Atmosphere Around the M-Dwarf Star GJ 436

C. D. Parkinson^{1,2} , S. W. Bougner³ , F. P. Mills^{1,4,5} , Y. L. Yung^{2,6}, A. Brecht⁷ , J. Li⁴, R. Hu⁶ , and G. Gronoff⁸ 

¹Space Science Institute, Boulder, CO, USA, ²Division of Geological and Planetary Sciences, California Institute of Technology, Pasadena, CA, USA, ³Climate and Space Sciences and Engineering Department, University of Michigan, Ann Arbor, MI, USA, ⁴Fenner School of Environment & Society, Australian National University, Canberra, ACT, Australia, ⁵McDonald Observatory, University of Texas Austin, Austin, TX, USA, ⁶Jet Propulsion Laboratory, California Institute of Technology, Pasadena, CA, USA, ⁷NASA Ames Research Center, Moffett Field, CA, USA, ⁸LARC-E303, Science Systems & Applications, Inc, Hampton, VA, USA

Abstract The chemical state of a Venus-like exoplanetary atmosphere depends on the far-ultraviolet (100–200 nm) to near-ultraviolet (NUV, 300–400 nm) flux ratio from the host star, the balance between CO₂ photolysis and recombination (which depends on water abundance), and catalytic chemical cycles. In this study, we use a three-dimensional (3-D) model to simulate conditions for a Venus-like exoplanet orbiting the M-dwarf star GJ436 by varying the ultraviolet (UV, <250 nm) and Near InfraRed (NIR, 0.7–5.0 μm) heating (Fels, 1977; National Research Council, 2000) to simulate a varying planet-star distance and considering the resultant effects on heating/cooling and dynamics. The simulation includes the upper mesosphere and thermosphere (<40 mbar). These simulations reveal that UV heating affects the energy balance, with both radiative and dynamical processes driving significant variations in zonal winds and global temperature profiles at pressures <10⁻⁵ mbar. More specifically, CO₂ 15-μm cooling balances UV and NIR heating at pressures >10⁻⁷ mbar with a strong maximum balance for pressures at ∼10⁻⁵ mbar, thus explaining the invariance of the temperature distribution at >10⁻⁵ mbar for all cases. Our simulations also show that moderate changes in the standard NIR heating (0.7× and 1.3×) result in relatively small changes in neutral temperature for pressures less than ∼10⁻⁵ mbar, and virtually no change for pressures greater than ∼10⁻⁵ mbar. However, with larger changes in the NIR heating profile (2× and 4×), much greater changes in neutral temperature occur throughout the altitude range studied.

Plain Language Summary Understanding an exoplanet's atmosphere depends on heat absorption, emission, gas mixing, and chemical interactions. However, only a few atmospheric gases can currently be detected via remote sensing techniques like spectroscopy—and only when they are abundant. Here, we use a three-dimensional model to simulate the atmosphere of a hypothetical Venus-like planet orbiting the M-dwarf star GJ 436. We examine how atmospheric temperatures, winds, and energy balance vary as the orbital distance decreases. A key result is that intense dayside heating in the upper atmosphere can produce emission features brighter than the surrounding thermal radiation. In particular, the 15-μm band of carbon dioxide (CO₂) may show a central brightness peak that stands out in the spectrum. Our simulations show how heating and cooling interact with atmospheric dynamics in dense CO₂-rich atmospheres around M-dwarfs. They also reveal distinct non-local thermodynamic equilibrium (NLTE) spectral features, caused when radiative processes outweigh local collisions in the upper atmosphere, disrupting equilibrium energy distributions. A key example is the 15-μm CO₂ dayside emission peak, driven by near-infrared and ultraviolet heating. Other NLTE features may arise in CO₂, O, and O₂ emissions under high extreme ultraviolet flux. These signals are critical for identifying Venus-like exoplanets and interpreting their stability and spectra.

1. Introduction

Atmospheric motion is an inescapable response to various forcings on a planet such as rotation, gravity, and differential stellar heating of the atmosphere. Dynamics describes the relationships among heating forces and the winds they drive. Dynamics can also affect a planet's climate and habitability. Winds, which are variable in time transport heat, which in turn affects atmospheric chemistry. Movement of air carries condensable species responsible for clouds, such as water on Earth and Mars, ammonia on Jupiter, methane on Titan, or sulfuric acid

on Venus. Dynamics also strongly affect the distribution of non-condensable trace gases. Generally, winds have a preferred direction that either persists seasonally or annually. Such climatological winds make up the general circulation of a planetary atmosphere. The role of atmospheric dynamics in the long-term evolution of atmospheres and planetary habitability remains relatively unexplored. Interpreting observations of terrestrial-like exoplanets and assessing their implications for comparative planetary evolution require understanding the chemical and physical processes in exoplanetary atmospheres.

Venus observations and models are two important sources of relevant information when studying dense CO₂-rich exoplanetary atmospheres. The theoretical understanding of these worlds is critical for the operation of observatories such as the James Webb Space Telescope (JWST) and the future very large (>30 m) ground-based observatories that will have an objective to study the habitability of planets. First, because Venus-like planets may be targets of interest in themselves (Kane et al., 2014, 2018, 2019, 2021; Way et al., 2016, 2023), but overall because it is important to understand why Venus is so different from Earth in terms of evolution. Hence, the objective of several JWST observations is to observe Venus-like atmospheres and understand the stability of these atmospheres in the light of their host stars. The thermal stability, partially driven by the wind patterns, is also an essential point to address. The observation of Venus-like exoplanets will also help better understand the history of the Earth, since the same processes that led to Venus' present atmosphere may have promoted the early habitability of the Earth (Turbet et al., 2021).

Several types of models have been used to study terrestrial-like exoplanets. 1-D photochemical (e.g., Harman et al., 2018) and radiative-convective models (e.g., Lincowski et al., 2018; Meadows et al., 2018; Mickol et al., 2015; Robinson & Catling, 2012; Robinson & Crisp, 2018) have been employed to simulate the global-average atmospheric composition and evolution of Venus-like exoplanets, including the upper atmospheric conditions and composition that will dominate observed spectra. 3-D General Circulation Models (GCMs) (e.g., Way & Del Genio, 2020) have been employed to simulate their bulk atmospheres.

Previous work using 1-D photochemical models has been published looking at the impact of the planet-star distance for Venus-like and/or Earth-like atmospheric compositions (Arney, 2019; Arney et al., 2017; Hu et al., 2020; Lincowski et al., 2018). They have been used frequently owing to their large potential parameter space to explore (e.g., Domagal-Goldman et al., 2014; Gao et al., 2015; Segura et al., 2005, 2007). While ideal for this purpose, these models have important inherent limitations. 1-D models simulate the vertical structure of a planetary atmosphere assuming horizontal uniformity, typically under globally averaged, diurnally averaged, or substellar point conditions. However, terminator regions—the boundary zones between day and night—exhibit steep horizontal gradients in temperature, pressure, composition, and radiation that cannot be resolved by horizontally averaged 1-D frameworks. In particular, a global-/diurnal-average simulation is not the same as what one would get from averaging over the global state of an atmosphere (e.g., Mills et al., 2021) and is not representative of the terminator region that a transit observation would sense; dynamical influences on species distributions are also ignored. 1-D radiative convective simulations can parameterize the effects of condensable species and clouds but suffer the same spatial limitations as 1-D photochemical models. 3-D GCMs allow for better interpretation of observations due to the multiple spatial dimensions being represented.

Exoplanet climate simulations have been performed previously with the Laboratoire de Meteorologie Dynamique-generic (LMD-G) Global Climate Model for a variety of cases (*viz.*, GJ 1132b, Trappist-1 planets, and Proxima Centauri b, Arney et al., 2016, 2017; Fauchez et al., 2019; Pidhorodetska et al., 2020; Turbet et al., 2018; Wordsworth et al., 2011). Details on the LMD-G GCM can be found by Turbet et al. (2018) and Fauchez et al. (2019). Like some GCMs used in exoplanet atmospheric research, the LMD-G GCM does not include photochemistry (Pidhorodetska et al., 2020). To simulate atmospheric composition, a 1-D photochemistry code is utilized to produce vertical chemical profiles separate from the LMD-G GCM. See details by Arney et al. (2016, 2017), Lincowski et al. (2018), Meadows et al. (2018), and review by Parkinson et al. (2021). Examples of other codes that have been used to do similar things include (a) ExoCAM, a modified version of the Community Atmosphere Model from NCAR, adapted for exoplanet simulations including tidally locked planets and diverse compositions (Wolf, 2017), (b) ROCKE-3D, a NASA GCM based on ModelE2 (Way et al., 2017), (c) Unified Model, a UK Met Office model that has been used for exploring atmospheric dynamics on a wide range of planets (Mayne et al., 2014), (d) THOR, a non-hydrostatic, 3-D GCM developed to explore atmospheres with deep convective motions and strong horizontal variations—often used for exoplanets with extreme heating (Mendonça et al., 2016), and (e) MITgcm, a flexible GCM originally designed for Earth's ocean and atmosphere,

but adapted to study exoplanet atmospheres including phase curves and hot spot offsets in tidally locked planets (Showman et al., 2013).

The 3-D Venus Thermospheric General Circulation Model (VTGCM) was designed for the study of Venus' middle and upper atmosphere (e.g., Bouger, Brecht, et al., 2015; Brecht et al., 2011, 2021; Parkinson, Gao, et al., 2015; Parkinson, Yung, et al., 2015; Parkinson et al., 2021) and can be used for exploring the portion of an exoplanetary atmosphere typically probed by transmission spectroscopy. In this initial study, we use the well-tested and validated (for a Venus context) VTGCM to simulate middle and upper atmosphere (<40 mbar) conditions on a Venus-like planet at varying distances from the M-dwarf GJ 436 and compare the results with those previously published for Venus. We believe these are the first 3-D simulations with consistent dynamics, energetics, and photochemistry focused on the observable middle and upper atmosphere of terrestrial exoplanets having thick CO₂-rich atmospheres (i.e., Venus-like exoplanets). Venus is a good proxy for an exoplanet study around M-dwarf stars since many close-in exoplanets are likely tidally locked in their orbits and Venus has a very slow rotational period, which approximates this well.

Several processes have been previously identified as important determinants of composition and chemistry in the observable upper atmosphere of an exoplanet: the ratio of far UV (FUV, 100–200 nm) and near UV (NUV, 300–400 nm) stellar radiation (e.g., Tian et al., 2014), total stellar FUV flux (e.g., Domagal-Goldman et al., 2014), and alternative catalytic chemical cycles (e.g., Gao et al., 2015; Grenfell et al., 2013). Recent modeling work has helped to reconcile earlier discrepancies regarding how stellar spectral properties affect photochemical pathways in dense CO₂-rich atmospheres. Harman et al. (2015) showed that increasing FUV flux while holding NUV constant only marginally increased O₂ concentrations, suggesting that reservoir species such as HO₂ and H₂O₂ play a buffering role in OH production. This insight was built upon by Harman et al. (2018), who introduced additional catalytic pathways and surface sinks, reducing the likelihood of abiotic oxygen false positives. Similarly, Hu et al. (2020) and Tian et al. (2014) refined the role of NUV-driven photolysis in regulating O₃ and HO_x cycling, particularly under M-dwarf spectral conditions. These developments provide a robust theoretical foundation for interpreting VTGCM photochemical outputs in this study and justify the spectral input selections and assumptions made herein. We have incorporated these processes using the VTGCM to perform investigations with coupled atmospheric energetics (heating/cooling), dynamics, and photochemistry (e.g., Parkinson et al., 2018).

1.1. The Influence of Stellar Characteristics

Multiple stellar characteristics can profoundly influence a planetary atmosphere. For instance, flares can produce bursts of energetic particles (SEPs) and enhanced UV radiation that may persist for hours to days, affecting mesospheric and thermospheric chemistry (Airapetian et al., 2016, 2019). While such effects have not been studied for dense CO₂-rich atmospheres, modeling efforts for thinner (Mars-like) and O₂-rich atmospheres suggest that flares are likely to drive only transient variations in atmospheric chemistry (Bouger, Pawlowski, et al., 2015; Pawlowski & Ridley, 2008, 2009a, 2009b; Segura et al., 2010).

GJ 436 does exhibit flare activity, but a recent analysis by Loyd et al. (2024) shows that these flares are unusually low in energy compared to other M dwarfs. The observed flare frequency distribution of GJ 436 exhibits a statistically significant lack of high-energy ($>4 \times 10^{28}$ erg) events, and the flares observed increased the star's time-averaged FUV output by only ~15% over nearly a full day of cumulative exposure. While these flares are frequent (minutes to hours), they do not resemble the intense outbursts typical of active mid- to late-type M dwarfs (Loyd et al., 2024).

More generally, although flaring is common on M dwarfs, the timescale of atmospheric radiative-dynamic equilibrium is much longer (weeks to months) than both the timescale of individual flare events (minutes to hours) and the frequency of all flare events, which ranges between 0.02 and 0.4 flares per hour for all M-dwarf spectral subtypes (M0–M6) (Kowalski et al., 2009). The frequency of large flare events would be much lower than this range. As a result, time-averaged steady-state models—like those used in this study—are more representative of the climatological mean state rather than transient perturbations. Even in more active M-dwarf cases, unless flare frequency is high enough to maintain a persistent bias in atmospheric forcing, short-duration flares are unlikely to alter the overall thermal structure or dynamics of the upper atmosphere in a sustained manner (Segura et al., 2010; Tilley et al., 2019). While typical M-dwarf flare rates range from 0.02 to 0.4 flares/hour (Kowalski

et al., 2009), only sustained high-frequency flaring over weeks to months would meaningfully enhance the time-averaged FUV flux enough to impact upper atmospheric structure or chemistry.

Therefore, we assume that both for GJ 436 specifically, and for typical stars that fall within the middle of the M spectral type range, flare events introduce only transient variability that does not deviate significantly from the climatological state of the atmosphere. This justifies their exclusion from the current simulations, which are focused on the long-term climatological state of a dense CO₂-rich exoplanetary atmosphere. Future work will explore time-dependent modeling and incorporate episodic high-energy events to address their possible transient and cumulative effects on composition and observables.

The FUV to NUV ratio and absolute intensity of FUV radiation may also have strong effects on the atmosphere, but previous simulations have yielded differing interpretations. Tian et al. (2014) suggested that a high FUV to NUV ratio was responsible for the buildup of O₂ because of decreased photolysis of O₃, H₂O₂, and HO₂ in their M-star case, and that the ratio of the O₃/H₂O₂/HO₂/H₂O photolysis to that of CO₂ was part of the driving phenomena. Harman et al. (2015) increased the FUV flux while holding the NUV flux constant, and found that higher FUV fluxes increased O₂ concentrations only slightly. Specifically, FUV photons are responsible for the photolysis of CO₂, producing free oxygen atoms that can recombine to form O₂. In contrast, NUV photons can destroy odd oxygen (O₃) and convert it to O₂ by supporting catalytic destruction cycles, such as those involving HO_x species. Therefore, a lower NUV-to-FUV flux ratio—as typically observed in M-dwarf stars like GJ 436—leads to a net buildup of O₂ due to reduced O₂ loss. Within this framework, both Tian et al. (2014) and Harman et al. (2015) emphasize that HO₂ and H₂O₂ act as reservoirs for OH, with their primary source being the photolysis of H₂O. Harman et al. (2015) showed that this H₂O photolysis is significantly suppressed—by a factor of 400—in their GJ 876 case compared to solar conditions due to reduced FUV flux. As a result, the relative concentrations of HO₂ and H₂O₂ are 2–3 orders of magnitude larger. However, neither study appears to have examined how the HO_x partitioning depends quantitatively on FUV and NUV fluxes. For instance, it remains unclear how important the O(¹D) + H₂O → 2OH reaction is in their models. This pathway is known to be a key source of OH in Earth's atmosphere, where O(¹D) is produced by O₃ photolysis. That said, both authors highlight the photochemical significance of the FUV/NUV flux ratio in M-dwarf stellar environments, where enhanced FUV-driven CO₂ photolysis and suppressed NUV-induced O₃ destruction can lead to elevated oxygen levels.

Similar unresolved differences exist regarding the impact of total FUV flux on O₂ and O₃ abundances. Domagal-Goldman et al. (2014) attributed O₃ buildup in their F-star case to higher FUV flux, but Harman et al. (2015) found substantially more O₂ in their simulation of a planet around a K-star than for a planet subject to the higher FUV flux orbiting an F-star, the opposite dependence of that from Domagal-Goldman et al. (2014). Harman et al. (2015) had nearly the same FUV/NUV ratio for both the K- and F-star in their pair of simulations. These issues were largely resolved by Harman et al. (2018), who showed that the FUV/NUV ratio, rather than the absolute FUV flux alone, governs the balance between O₂ production and destruction, and by Hu et al. (2020), who used coupled climate-photochemistry models to demonstrate that atmospheric composition and radiative transfer must be considered self-consistently to correctly predict O₂ and O₃ abundances under varying stellar spectra.

In the case of the current study, we assume that the host M-dwarf is quiet enough to not photodissociate all the CO₂ in the upper atmosphere through flares and particle precipitation; however, the stellar extreme ultraviolet (EUV)-XUV flux is still considered. We verify that, under these assumptions, enough CO₂ is present in the thermosphere to cool it down for negligible (i.e., Venus-like) atmospheric escape.

GJ 436 is an M2.5V star whose characteristics have been observed extensively, partly due to the discovery of GJ 436b, a Neptune-sized planet orbiting it (e.g., Butler et al., 2004; von Braun et al., 2012). Its spectrum has been measured at UV (France et al., 2013) and Near Infrared (NIR) (Terrien et al., 2015) wavelengths and its FUV/NUV ratio is high compared to that of the Sun. The GJ 436 spectrum has been used in several previous exoplanet simulations (e.g., Gao et al., 2015; Harman et al., 2018; Segura et al., 2003). The actual exoplanet GJ 436b is a Neptune like planet thought to be in a state of hydrodynamic escape (Ehrenreich et al., 2015) since a large cloud of H₂ has been observed in its vicinity. However, for a planet with a Venus-like atmosphere orbiting GJ 436, the depletion of H-containing species means that we can have a more stable CO₂-rich atmosphere with higher-mass constituents. As we will see in the following, cooling by CO₂ should prevent the atmosphere from being in a hydrodynamic-escape state.

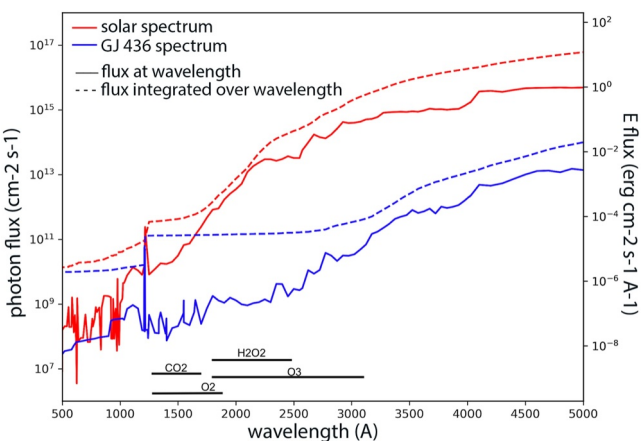


Figure 1. The Sun's spectrum (WMO, 1985; red) and GJ 436 photon flux, integrated photon flux, and energy flux (from the MUSCLES Hubble Space Telescope Treasury survey, binned to the JPL/Caltech KINETICS grid). Values are scaled such that the total flux of each is the same as the total flux received at 1 AU ($\sim 1,360 \text{ W m}^{-2}$) (Gao et al., 2015; Tian et al., 2014). The wavelengths at which photolysis of key species of astrobiological significance (viz., CO_2 , O_2 , O_3 , and H_2O_2) is most efficient are added for comparison (Tian et al., 2014). GJ 436 is brighter in the IR and contributes to the normalization of the total flux to $1,360 \text{ W m}^{-2}$.

1.2. Heating, Cooling, and Dynamics

The ability of photochemical processes to influence broad regions of an atmosphere depends on transport, which is controlled by differential heating and cooling in the atmosphere. On present day Venus (and ancient Mars), the dayside heat budget is (was) dominated by a balance of EUV heating and CO_2 15- μm cooling above the NIR heating layer (e.g., Bouger et al., 1999, 2002; Parkinson et al., 2021; Valeille et al., 2009, 2010). For present day Mars and Earth, CO_2 15- μm cooling plays a different but still important role in the heat budget (e.g., Bouger et al., 2002). Photolysis of CO_2 and O_2 generates a large quantity of atomic O, increasingly so for present day Venus over Mars (the former being closer to the sun), and for ancient Mars (when solar EUV-UV fluxes were much higher). Subsequent O- CO_2 collisions pump up the first CO_2 vibrational level, thereby enhancing CO_2 cooling where the timescale for collisional de-excitation exceeds the timescale for the emission of a 15- μm photon (e.g., Bouger et al., 1999, 2017; Parkinson et al., 2021). For Venus, this strong CO_2 15- μm cooling also becomes increasingly important as the solar cycle advances (from solar minimum to maximum conditions), thereby enhancing dayside O abundances and producing larger CO_2 cooling rates. This O- CO_2 regulated “thermostat” yields a rather weak solar cycle variation in dayside upper thermosphere temperatures on Venus ($\sim 70 \text{ K}$), much smaller than on either Earth or Mars (Bouger et al., 1999). This “thermostatic” effect has important implications for our GJ436 exoplanet model results as well (see Section 3).

Spectra of GJ 436 (cf., Figure 1) from the Hubble Space Telescope (HST) Measurements of the Ultraviolet Spectral Characteristics of Low-mass Exoplanetary Systems (MUSCLES) Treasury Survey indicate reduced stellar fluxes (with respect to our Sun) in the spectral region where atmospheric CO_2 , H_2O_2 , O_2 , and O_3 photolysis occurs (Gao et al., 2015; Tian et al., 2014). In the context of photochemically active wavelengths, for a constant planet-star distance, F-type stars emit more flux than G-type stars in the near-ultraviolet and far-ultraviolet bands, while K and M dwarfs emit significantly less flux in both ranges. The reduction is especially pronounced in the NUV, which is critical for photolysis of molecules like H_2O_2 , HO_2 , and O_3 . This spectral contrast leads to slower destruction of ozone and hydrogen oxide radicals around cooler stars and potentially allows photochemically generated ozone to accumulate (Harman et al., 2015; Segura et al., 2005). These effects are important when interpreting upper atmospheric temperature structure and radiative cooling, as modeled in this study. H_2O , O_2 , and CO_2 photolysis is driven by FUV photons whereas H_2O_2 , HO_2 , and O_3 photolysis is driven by NUV photons. This should mean less atomic O production, leading to reduced CO_2 15- μm cooling and warmer upper atmosphere temperatures (above any near IR heating layer), for Venus-like planets around K and M class stars despite their smaller heating rates. We discuss exo-Venus modeling simulation results in Section 3, where we examine the impact of EUV-UV and NIR heating on the energy balance and dynamics for a dense CO_2 -rich exoplanetary atmosphere.

2. Numerical Modeling Tool: VTGCM

The VTGCM is a 3-D finite difference hydrodynamic model of Venus' upper atmosphere developed from NCAR's terrestrial Thermosphere Ionosphere GCM (TIGCM) (e.g., Bouger et al., 1988). The VTGCM solves the time-dependent primitive equations for a neutral upper atmosphere. Additionally, the prognostic equations (thermodynamic, eastward and northward momentum, composition) are typically solved for steady-state solutions for the temperature, zonal and meridional velocities, and the mass mixing ratios of specified major and minor species (e.g., Bouger, Pawlowski, et al., 2015; Bouger, Jakosky, et al., 2015; Bouger, Bell, et al., 2015; Brecht et al., 2011, 2021; Parkinson, 2021). This model has been documented in detail as revisions and improvements have been made over more than three decades including modern parameterizations for CO_2 15- μm cooling, NIR heating, wave drag, and eddy diffusion enabling the VTGCM to reproduce many *Pioneer Venus Orbiter* (PVO) and *Venus Express* (VEx) observations, including solar cycle effects and nightglow intensities (e.g., Bouger et al., 1986, 1988; Bouger, Pawlowski, et al., 2015; Bouger, Jakosky, et al., 2015; Bouger, Bell, et al., 2015; Brecht et al., 2011, 2012, 2021; Gilli et al., 2015). These previous VTGCM modeling efforts for

Table 1*Extreme Ultraviolet/Ultraviolet Flux Variation Simulations: Changing by Reducing Star-Planet Distance*

Case	Stellar flux	Planet-star distance (AU)	Equilibrium temperature, T_{eq} (K)	Comments
VEN1	Sun (s_{min})	0.72	~230 (Venus, solar min.)	Venus Baseline
VEN2	GJ 436	0.72	~90 (GJ 436)	Fluxes change only
VEN3	GJ 436	0.38	~140 (GJ 436)	Fluxes and Planet-star distance
VEN4	GJ 436	0.175	~185 (GJ 436)	Fluxes and Planet-star distance

Venus' upper atmosphere (e.g., Bougner, Bell, et al., 2015; Bougner, Jakosky, et al., 2015; Bougner, Pawlowski, et al., 2015; Brecht & Bougner, 2012; Brecht et al., 2011, 2012; Ledvina & Brecht, 2020; Parkinson et al., 2021) are directly relevant to the analogous exoplanet research performed in this paper.

The VTGCM model domain covers a 5° by 5° latitude-longitude grid with 69 evenly spaced log-pressure levels in the vertical, extending from ~ 70 to 300 km (~ 70 –200 km) at local noon (midnight). This middle and upper atmosphere domain corresponds to pressures $<\sim 40$ mbar. Differences in altitude coverage between the dayside and nightside arise because the hotter dayside atmosphere has a larger scale height and is therefore more vertically extended, necessitating a higher model top to capture the thermospheric structure (e.g., Bougner, Bell, et al., 2015; Bougner, Jakosky, et al., 2015; Bougner, Pawlowski, et al., 2015). The adopted altitude/pressure range ensures that all the dynamic influences contributing to the NO, O₂, and OH nightglow layers can be captured, and the wave processes above the cloud top region can be addressed. Furthermore, the VTGCM solar flux bins can capture the full range of EUV-FUV flux conditions (~ 1 –250 nm). Finally, observational comparisons show that the VTGCM closely matches Venus' climatological circulation (e.g., Bougner, Bell, et al., 2015; Bougner, Jakosky, et al., 2015; Bougner, Pawlowski, et al., 2015), so we use the present VTGCM dynamical scheme for the 3-D energy balance studies in this paper.

The VTGCM includes a simplified photochemical treatment that captures the major dynamical and radiative effects of neutral species in the upper atmosphere. Within the model, species are grouped by their roles: major species (CO₂, CO, O, N₂) directly influence the atmospheric mean mass, temperature, and global-scale winds; minor species (O₂, N⁴S, N²D), NO, SO, SO₂) are included diagnostically and contribute to radiative cooling and compositional gradients but do not feedback on dynamics; additional chemical tracers (e.g., Cl, Cl₂, ClCO, ClO, H₂, HCl, H₂O, HO₂, H₂O₂, O₃, OH) are incorporated via vertical profiles from an altitude of ~ 70 –110 km (from the 1-D JPL/Caltech KINETICS model; Zhang et al., 2010, 2012). These species are subject to photolysis under solar UV/EUV forcing, and their presence influences heating and cooling rates, especially in Venus' middle atmosphere. The VTGCM accounts for altitude-dependent solar heating, molecular diffusion, and radiative cooling by CO₂ and other species, providing a consistent framework for simulating the coupled photochemical-dynamical structure of the upper atmosphere. Prior applications of the VTGCM to Venus have validated its performance against spacecraft data (e.g., Bougner, Bell, et al., 2015; Bougner, Jakosky, et al., 2015; Bougner, Pawlowski, et al., 2015; Brecht et al., 2021; Parkinson et al., 2021) and these studies have shown that the model captures key processes relevant to the non-equilibrium and steady-state chemistry of high-altitude layers. See Parkinson et al. (2021) for further details of photochemistry.

Output from the Flexible Modeling System Venus GCM (Lee & Richardson, 2010; Lee et al., 2011) is used to define a lower boundary that is a good representation of the connection between the lower and upper atmospheres (Brecht et al., 2021). The VTGCM is used in this study to conduct preliminary exoplanet simulations for conditions around the M dwarf star GJ 436 at various star-exoplanet distances (*cf.*, Table 1). Steady state solutions have been obtained by solving the thermal, dynamical, and chemical equations consistently.

3. VTGCM Simulations: Energy Balance Results and Discussion

Simulation Design: This study uses the VTGCM to explore how variations in stellar flux affect the thermal structure and dynamics of a dense CO₂-rich atmosphere for a Venus-like planet orbiting the M-dwarf star GJ 436. We performed four simulations (VEN1–VEN4), each designed to isolate different components of the stellar radiative input. Section 3.1 focuses on the effects of varying the EUV–UV heating component using observed spectra for two stellar types: the Sun (VEN1) and the M-dwarf GJ 436 (VEN2–VEN4) and then decreasing the

planet-star distance (VEN3 and VEN4). In these cases, the NIR heating rate is held constant to isolate the impact of shorter wavelength flux. Section 3.2 extends this investigation by incrementally increasing the NIR heating in two additional simulations (VEN4a and VEN4b), representing 2 \times and 4 \times enhancements in near-infrared flux relative to VEN4. This stepwise approach allows us to distinguish the atmospheric response to UV versus IR radiation under consistent planetary and model boundary conditions. All simulations assume steady-state forcing, fixed planetary parameters (e.g., radius, mass, Venus-like rotation), and use stellar fluxes scaled to preserve bolometric consistency. Labels for each simulation case (VEN1–VEN4, VEN4a, and VEN4b) are indicated in figures and text throughout Section 3.

3.1. Impact of EUV-UV Heating on Energy Balance

Figure 1 shows a comparison between the solar spectrum (WMO, 1985), and a spectrum of the M dwarf GJ 436 from the MUSCLES HST Treasury survey, binned to the standard JPL/Caltech KINETICS wavelength grid. In this figure, the fluxes are scaled so that the total flux equals the total solar flux at 1 AU, \sim 1,360 W m $^{-2}$. The wavelengths at which photolysis of CO₂, O₂, O₃, and H₂O₂ is most efficient are added for comparison (Tian et al., 2014). Recent observations of several planet-hosting M-dwarfs show that most have FUV/NUV flux ratios 1,000 times greater than that of the Sun (Tian et al., 2014), and so the relative photolysis rates of key species (e.g., CO₂ and O₃) will differ between the two cases. We regard the GJ 436 spectrum to be fixed in the simulations and do not consider variable phenomena such as flares in our study. Note that while the plotted GJ 436 stellar flux in Figure 1 extends to 400 nm, the VTGCM currently includes photolytic and heating effects only for wavelengths \leq 250 nm. Thus, key photolytic pathways involving O₃, which presents an absorption cross-section extending out to 310 nm, are likely underrepresented in our current model configuration.

The M dwarf GJ 436 stellar EUV/FUV fluxes were utilized in conjunction with various star-exoplanet distances for a suite of Venus-like exoplanet simulations (see Table 1). The estimate of the equilibrium temperatures for each case (third column) is given by the formula:

$$T_{\text{eq}} = \left(\frac{(1 - A)L_*}{16\pi\sigma d^2} \right)^{0.25}$$

where A is the Bond albedo (Venus \approx 0.77), L_* is the stellar luminosity of GJ 436 (2.5% of the sun, d is the orbital distance, and σ is the Stefan-Boltzmann constant, Torres et al., 2008; von Braun et al., 2012). The resulting exoplanet geopotential heights, neutral temperatures, heat balances, and cross-terminator zonal winds for the various cases considered are shown in Figures 2, 3, 5 and 6, respectively. Panel (a) in all these figures corresponds to VEN1, our baseline Venus case. All panels (b)–(d) (VEN2–VEN4) use GJ 436 stellar fluxes. For all panels (b)–(d), only the planet-star distance is changed as indicated in Table 1 with no other changes. The VTGCM baseline case run is for solar minimum conditions corresponding to the most recent *Venus Express* (VEx) observations (Bougher, Pawlowski, et al., 2015; Bougher, Jakosky, et al., 2015; Bougher, Bell, et al., 2015) with upgraded O_x, SO_x, HO_x chemistry (Mills et al., 2021). These multi-panel figures vividly show the initial comparison of a Venus-like exoplanet versus modern Venus for various planet-star distances from the parent star.

Figure 2 shows that the geopotential heights in panels (b) and (c) have some dayside upper atmospheric differences but generally do not vary much from the Venus baseline case shown in panel (a). However, for the closest planet-star distance to GJ 436 (panel (d)), we clearly see a maximum dayside geopotential height of 550 km as compared to a nightside geopotential height of \sim 220 km. This means that the atmosphere is inflating or bulging due to intense EUV-UV heating on the dayside. Global average heights at a given pressure level are shown on the right-hand side of each plot.

It is seen in Figure 3 that the VTGCM simulations have much faster winds for all cases on the evening terminator (ET) than on the morning terminator (MT), located at 18 and 6 h respectively. The maximum MT and ET wind speeds are tabulated in Table 2, and we see that the wind speed more than doubled for our VEN4 case and is remarkably fast at the ET. This can be understood by examining Figure 4 which shows the Venus upper atmosphere mean circulation paradigm adopted from Brecht et al. (2011). Here, the sign convention is understood by making use of Figure 4. A “+” zonal wind indicates the same direction as the planetary rotation (and additive for the superrotating zonal winds at ET) and “−” indicates zonal wind opposite to the planetary rotation (and opposing the superrotating zonal winds at MT). Previous observations show that Venus' upper atmosphere has

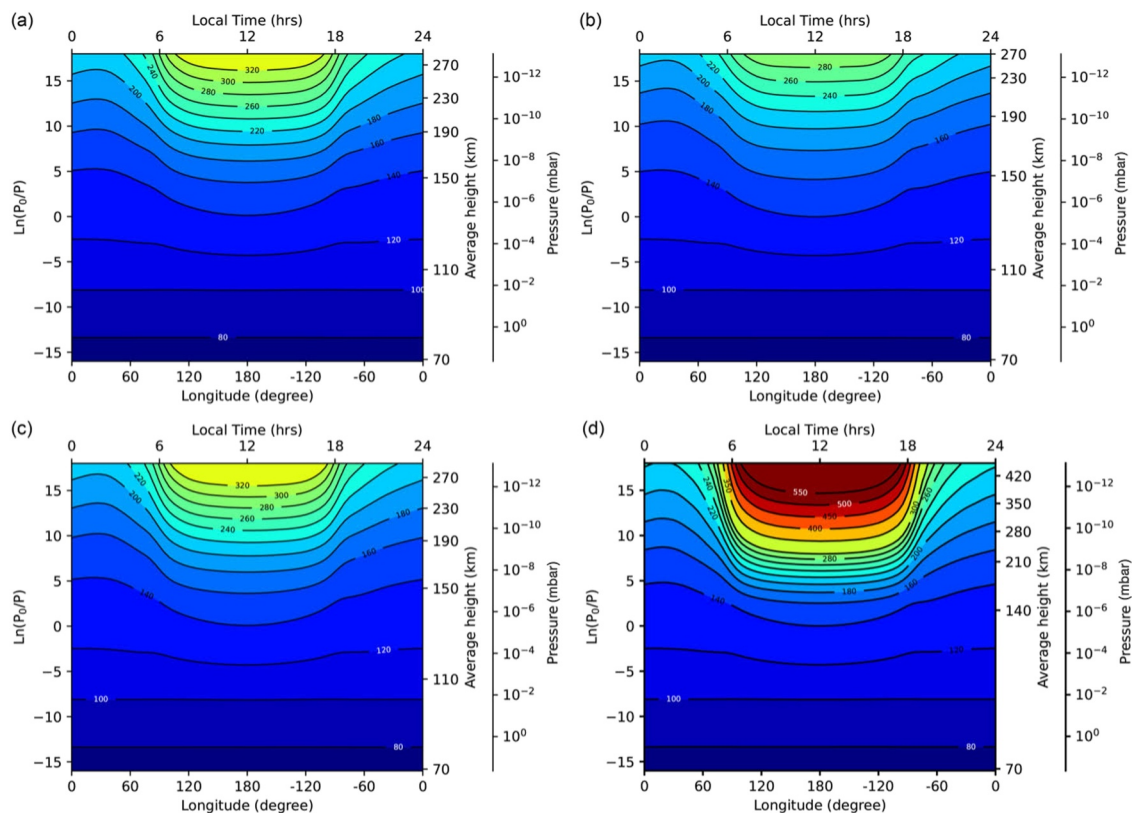


Figure 2. Geopotential Height. Panel (a) VEN1: shows the present-day Venus Thermospheric General Circulation Model (VTGCM) baseline case for solar minimum conditions (validated against Venus Express observations); panel (b) VEN2: VTGCM GJ 436 Venus at $d = 0.72$ AU (present Venus orbital distance); panel (c) VEN3: VTGCM GJ 436 Venus at $d = 0.387$ AU (present Mercury orbital distance); panel (d) VEN4: VTGCM GJ 436 Venus at $d = 0.175$ AU (closest orbital distance). All panels are at 2.5°N latitude (equatorial).

two dominant circulation flow patterns (e.g., Bouger et al., 1997, 2006; Brecht et al., 2021; Lellouch et al., 1997; Schubert et al., 2007). The flow known as the retrograde superrotating zonal flow (RSZ) occurs in the region from the surface of the planet to above the top of the cloud deck (~ 70 km) and then emerges again in the thermosphere. This region is dominated by a wind pattern flowing in the direction of the planet's spin and is faster than Venus' rotation. Zonal winds up to ~ 100 – 140 m/s are seen near cloud tops. The second flow pattern occurs above ~ 120 km and is a relatively stable mean subsolar-to-antisolar flow (SS-AS) (Bouger et al., 1997). In the upper atmosphere, Venus has inhomogeneous heating driven mainly by solar radiation (EUV, UV, and IR) thus inducing large pressure gradients to generate the dominant SS-AS flow pattern (Bouger et al., 1997; Dickinson & Ridley, 1977; Schubert et al., 1980). The transition region is defined as the altitude range of 70 – 120 km where the RSZ and SS-AS circulation patterns overlap and are presumed superimposed (e.g., Bouger, Pawlowski, et al., 2015; Bouger, Jakosky, et al., 2015; Bouger, Bell, et al., 2015). This means that both flows can be alternately dominant in this altitude region and observations suggest a high degree of variability of these wind components in the transition region (Brecht et al., 2011, 2021).

The net effect of this general flow pattern paradigm in the upper atmosphere causes (a) a shift in the divergence of the flow from the subsolar point toward the ET, (b) stronger ET winds than those along the MT, and (c) a shift in the convergence of the flow away from midnight and toward the MT (Schubert et al., 2007). This general flow pattern also applies to our exo-Venus case as shown in Figure 3. It is easy to see that the situation varies with altitude, reflecting the changing importance of the underlying drivers and possible solar cycle variations.

A comparison of the Venus baseline case (VEN1) and that for GJ 436 fluxes at 0.72 AU (VEN2) shows that: (a) dayside upper thermosphere temperatures ($< 10^{-7}$ mbar) (Figure 5a vs. 5b) are up to ~ 30 K cooler for VEN2, and (b) nightside temperatures are similar. This reduced temperature difference in the dayside upper thermosphere arises because the EUV–FUV flux from GJ 436 is significantly lower than that of the Sun, resulting in reduced

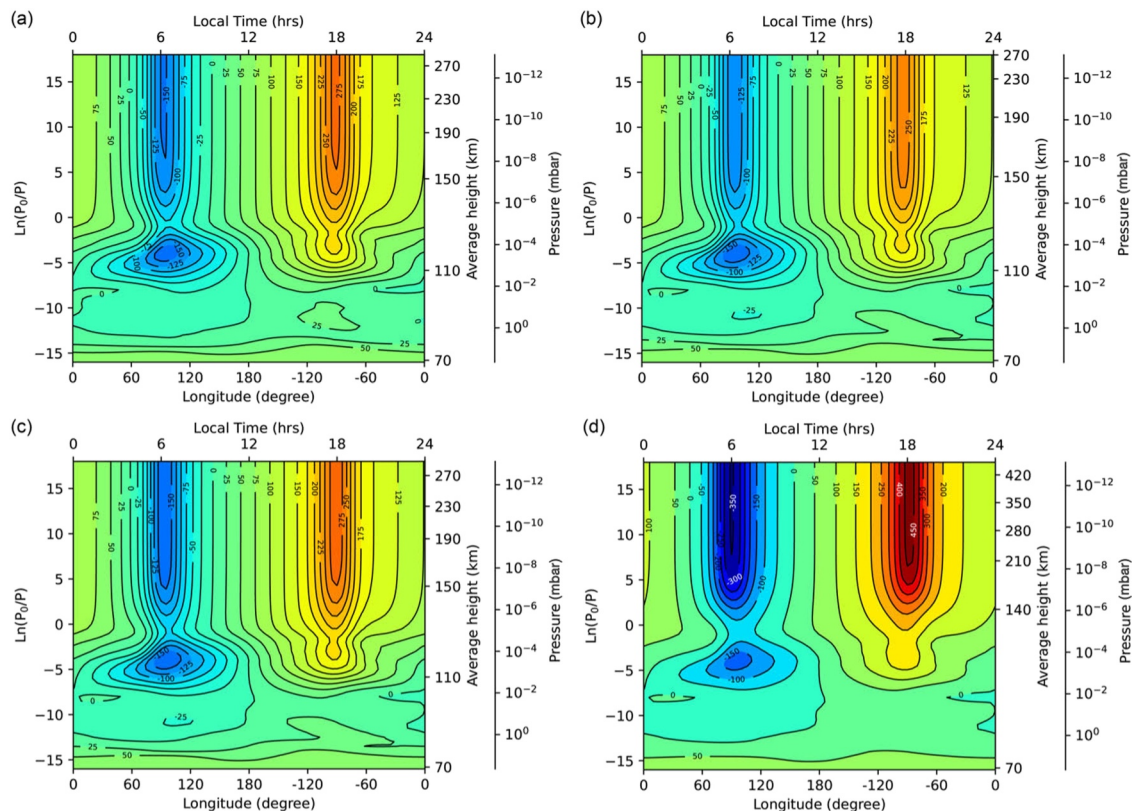


Figure 3. $u(z)$ Zonal Wind. Panel (a) **VEN1**: shows the present-day Venus Thermospheric General Circulation Model (VTGCM) baseline case for solar minimum conditions (validated against Venus Express observations); panel (b) **VEN2**: VTGCM GJ 436 Venus at $d = 0.72$ AU (present Venus orbital distance); panel (c) **VEN3**: VTGCM GJ 436 Venus at $d = 0.387$ AU (present Mercury orbital distance); panel (d) **VEN4**: VTGCM GJ 436 Venus at $d = 0.175$ AU (closest orbital distance). All panels are at 2.5°N latitude (equatorial). m s^{-1} units are used throughout the study. The sign convention is defined in Table 2 caption.

heating of the upper thermosphere on the dayside in the VEN2 case. In contrast, the nightside thermospheric temperatures remain similar between VEN1 and VEN2, as they are largely governed by downward conduction and dynamic redistribution rather than direct stellar input. The latter indicates that the nightside is largely isolated from the dayside. This isolation is characteristic of a planet with efficient energy loss mechanisms in the upper atmosphere that is rotating sufficiently slowly for it to be close to being tidally locked. Corresponding comparisons among the Venus baseline case (VEN1) and those for GJ 436 fluxes at ~ 0.38 AU (VEN3) and ~ 0.175 AU (VEN4) importantly show that: (a) dayside upper thermosphere temperatures (Figures 5c vs. 5d, respectively) warm by ~ 25 and 345 K over the Venus baseline case, and (b) nightside temperatures are much the same (isolated from the dayside), which affirms that nightside energy is provided by atmospheric circulation rather than radiation. The VEN3 case at the Mercury planet-star distance with the GJ 436 fluxes yields Venus-like current temperatures (i.e., for solar minimum conditions). For all cases thus far, the simulated temperatures are much the same for pressures $> 10^{-5}$ mbar (where near IR heating is more important than EUV/FUV heating and cooling occurs predominantly via CO_2 15- μm emission). To understand this, we must examine the energy balance for each case. Comparing Figures 3 and 5, we note that at/above about 130 km the slower wind speeds at the MT correlate with a steeper temperature gradient at the MT, contrary to the faster wind speeds and less steep temperature gradient at the ET for all cases VEN1–VEN4.

In Figure 6, we see that EUV/UV heating and conductive cooling are the dominant heating/cooling terms for pressures $< 10^{-7}$ mbar for all cases, roughly balancing each other. We emphasize here that the near IR (NIR) heating is held constant for each case to isolate the effects of increased EUV/UV heating arising from moving the exoplanet closer to GJ 436. We remark that for the Venus baseline case (VEN1) was for solar minimum conditions. If we had considered conditions for solar maximum, such as was the case for *Pioneer Venus Orbiter* (PVO), NIR heating would have been the same as shown but the EUV/UV heating would be about double that

Table 2

Ultraviolet (UV) Flux Variation Study: Various Parameters From Figures 2, 3, 5, and 6

Case	Max geopotential height near equator (km) and noon: midnight atmospheric elongation ratio	Dayside T_{exo} noon near equator (K)	Max MT versus ET winds near equator (m/s)	Max dayside CO ₂ 15-μm cooling and EUV/ UV/IR heat balance ^a (K/day)
VEN1	320 (~3:2)	246	-150/+275	3,000
VEN2	280 (~3:2)	210	-125/+250	2,500
VEN3	320 (~3:2)	270	-150/+275	3,000
VEN4	630 (~5:2)	620	-350/+450	12,000

Note. Sign convention is “+” for the same direction as the planetary rotation (and additive for the superrotating zonal winds at ET) and “−” opposite to the planetary rotation (and opposing the superrotating zonal winds at MT). See Figure 4 diagram. ^aAll days are terrestrial days.

used for panel (a). The localized enhancement in conductive cooling at $\ln(dP_0/dP) = 0$ is positive causing dT/dz to reverse sign and push heat upward instead of downward causing the upper atmosphere to heat up more for larger values. This is the pressure at which the CO₂ 15-μm band becomes opaque so it can't radiatively cool and therefore convection becomes important for vertical energy transport. A positive dT/dz indicates heat is conducted downward, while a negative dT/dz indicates heat is conducted upward; localized heating occurs near regions where dT/dz approaches zero. CO₂ 15-μm cooling balances EUV/UV and NIR heating for pressures $>10^{-7}$ mbar with maximum cooling that completely balances the EUV/UV and NIR heating at pressures $\sim 10^{-5}$ mbar, thus explaining the invariant temperature distribution at pressures of 10^{-5} to 10^{-3} mbar for all cases. These dayside temperatures ($T_{\text{exo}} \sim 270$ K) would be much warmer than predicted here if the CO₂ 15-μm cooling was not enhanced by collisions of O and CO₂ (see Section 1.1). In short, the enhanced non-LTE CO₂ 15-μm cooling provides a strong thermostat that helps to regulate dayside temperatures for pressures of 10^{-7} to 10^{-2} mbar (e.g., Bouger et al., 2002) for the cases shown thus far.

3.2. Impact of NIR Heating on Energy Balance

In this study, the NIR heating profile was not recalculated dynamically for each new level of stellar NIR flux but instead scaled uniformly based on multiplicative increases. While this approach does not capture potential feedback between atmospheric structure and NIR absorption—such as changes in optical depth or the absorption profile (leading to significant changes in heating at lower altitudes), cloud formation, or re-radiation—it enables a

controlled NIR heating sensitivity analysis. The NIR flux should scale with $1/R^2$ just like the UV flux (National Research Council, 2000; Rypdal, 2017), and Figure 7 illustrates how we parameterize this in our model by using a multiplicative scaling factor with the standard Venus profile. Illustrated in this figure are the various NIR heating profiles used for the VTGCM GJ 436 Venus ($d = 0.175$ AU) NIR heating sensitivity study, obtained by multiplying the standard reference Venus NIR profile at 0.72 AU by various multiplicative factors. The larger the multiplicative factor, the greater the corresponding increase in the NIR heating, parameterizing a range of decreasing Planet-Star distances. Fujii et al. (2017) suggest that the stratospheric dynamical response to increased stellar radiation is similar for stars of different spectral types, but for a warmer star, the onset of strong upward motion occurs at a much larger incident flux because less of the installation is in the NIR where the radiation is more efficiently absorbed by water vapor and clouds. However, a higher temperature star (if it's emitting like a blackbody) will have a smaller fraction of flux in the NIR but the absolute flux will be larger because a warmer blackbody has higher absolute emission at all wavelengths. Shown in Figure 7 are the standard reference NIR and 0.7×, 1.3×, 2.0×, and 4.0× the standard reference NIR heating profiles. This represents a first-order approximation of the atmospheric response to enhanced NIR flux and is consistent with sensitivity studies used in prior modeling efforts (e.g., Brecht et al., 2021). We reiterate that although this method does not capture possible feedback between heating and atmospheric composition or structure, it allows us to isolate

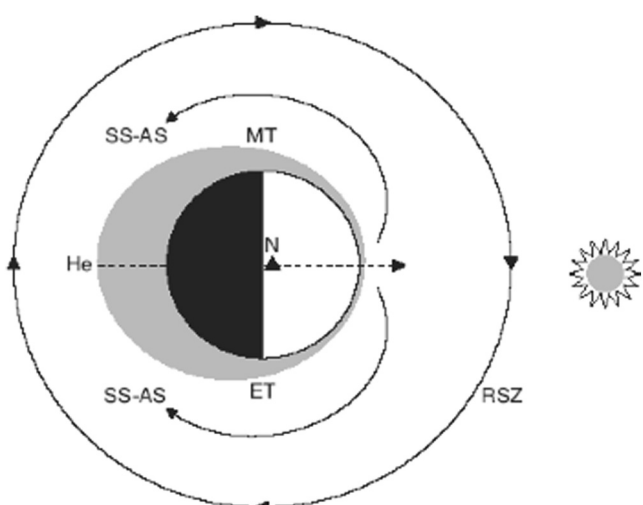


Figure 4. Simple Venus upper atmosphere circulation paradigm. Here, MT = morning terminator; ET = evening terminator; SS-AS = stable subsolar to antisolar circulation cell driven by NIR and EUV heating; RSZ = retrograde superrotating zonal flow that seems to vary greatly over time; and He = helium tracer bulge. Adopted from Brecht (2011).

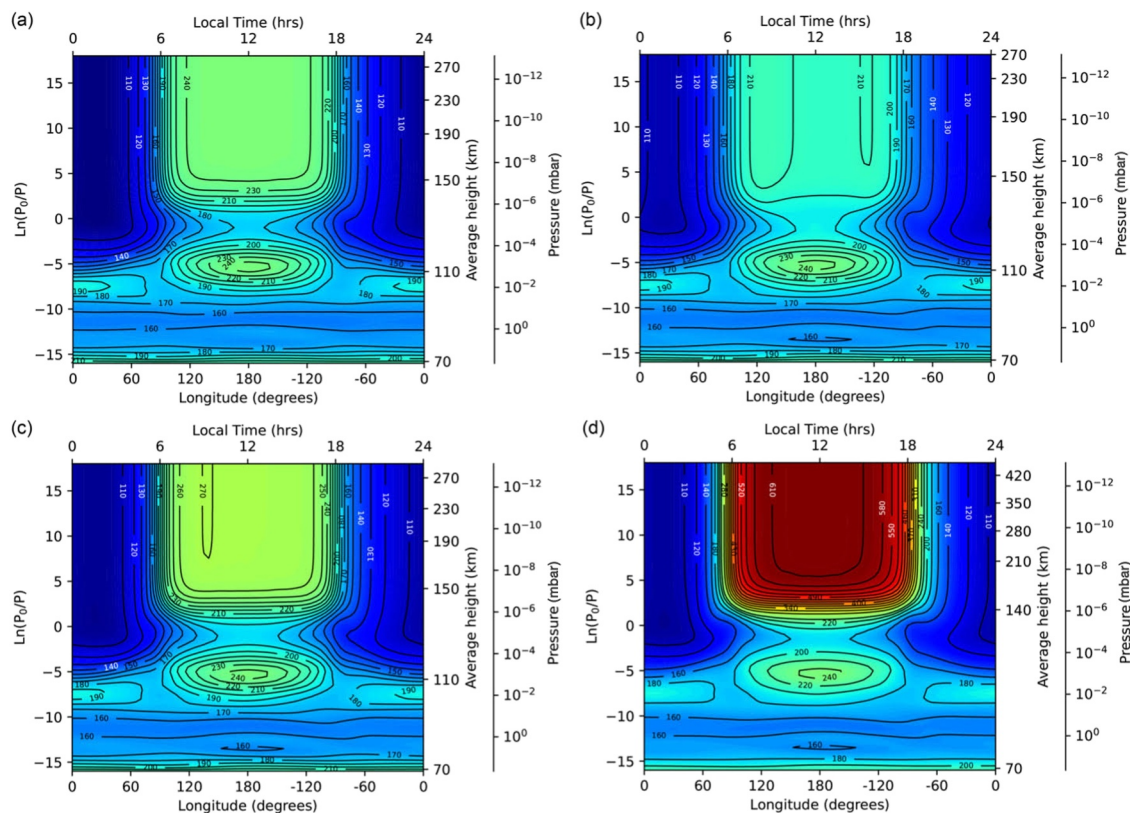


Figure 5. Neutral Temperature. Panel (a) **VEN1:** shows the present-day Venus Thermospheric General Circulation Model (VTGCM) baseline case for solar minimum conditions (validated against Venus Express observations); panel (b) **VEN2:** VTGCM GJ 436 Venus at $d = 0.72$ AU (present Venus orbital distance); panel (c) **VEN3:** VTGCM GJ 436 Venus at $d = 0.387$ AU (present Mercury orbital distance); panel (d) **VEN4:** VTGCM GJ 436 Venus at $d = 0.175$ AU (closest orbital distance). All panels are at 2.5°N latitude (equatorial). Kelvin (K) units are used throughout.

the dynamical and thermal consequences of increased NIR forcing in a controlled and interpretable framework. Future work will incorporate spectrally resolved self-consistent NIR heating computations to address this limitation. Therefore, this scaling should be interpreted as a first-order approximation that isolates the thermal and dynamic impacts of enhanced NIR forcing.

Figure 8 shows the energy balance for the four cases of the NIR sensitivity study for VEN4 in panels (a), (b), (c), and (d), respectively. Kelvin (K)/day units are used for each panel in the figure. As before (*cf.*, Figure 6), we see that EUV/UV heating and conductive cooling are the dominant heating/cooling terms for pressures $<10^{-7}$ mbar for all cases. The second thing to note in this figure is that moderately large changes of $\pm 30\%$ in the NIR heating profiles corresponding to panels (a) and (b) do not seem to cause much change in the CO_2 15- μm cooling profile, although a minor decrease/increase is seen at 10^{-4} mbar for each case compared to Figure 6 panel (d). However, when the NIR heating profile is doubled and quadrupled, the CO_2 15- μm cooling progressively compensates, attempting to maintain the energy balance, as seen in panel (d) where the NIR heating profile maximum matches that of the EUV/UV heating higher in the atmosphere. So, it is seen that enhanced non-LTE CO_2 15- μm cooling still provides an effective thermostat which helps to regulate dayside temperatures for pressures of 10^{-7} to 10^{-2} mbar even with very large changes in the NIR heating profile.

One might ask the following: (a) what is the impact on the energy balance of increasing the NIR heating profile as shown in Figure 8, that is to say, just how effective is the enhanced non-LTE CO_2 15- μm cooling, and (b) how much does altering the energy balance by dumping this extra NIR energy throughout the pressure range shown affect key atmospheric parameters for a close-in planet with a dense CO_2 -rich atmosphere orbiting an M-dwarf star? Figures 9–11 show how changes to the NIR heating/energy balance affect the geopotential height, zonal wind, and temperature profiles, respectively. In each of these figures, Panel (a, VEN1) represents Venus VTGCM base case for solar minimum conditions (validated against Venus Express observations); panel (b, VEN2) VTGCM GJ 436

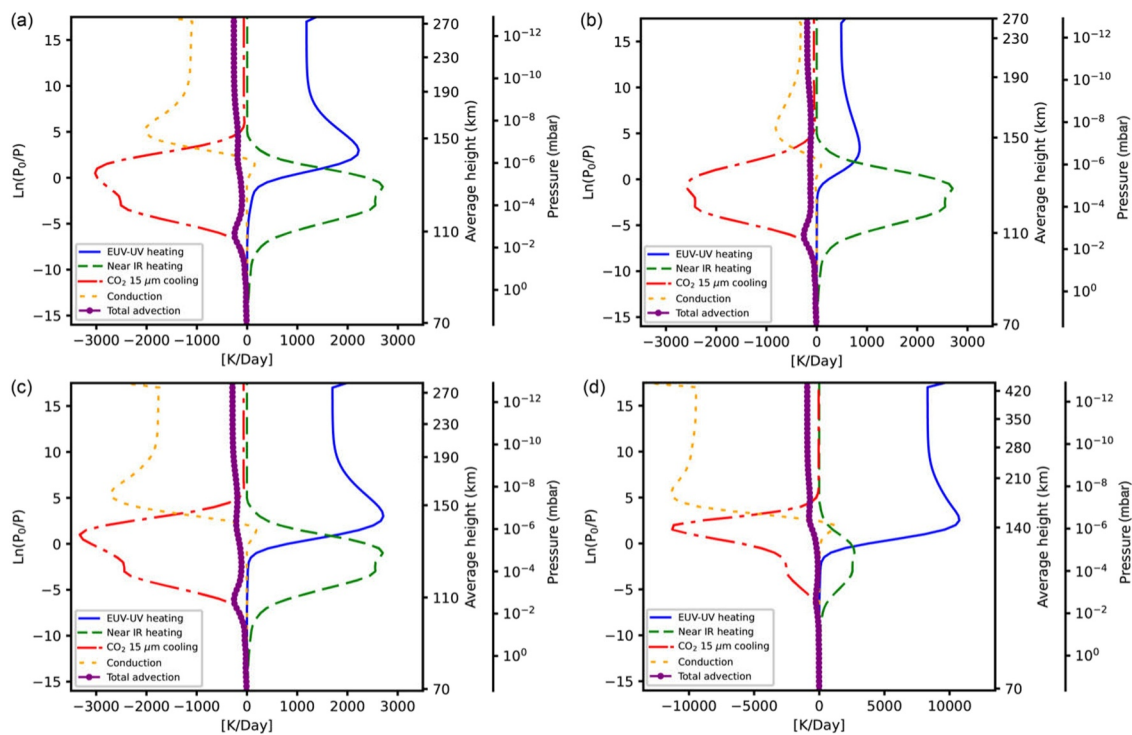


Figure 6. Energy balance analysis with Venus NIR heating constant. Panel (a) VEN1: shows the present-day Venus Thermospheric General Circulation Model (VTGCM) baseline case for solar minimum conditions (validated against Venus Express observations); panel (b) VEN2: VTGCM GJ 436 Venus at $d = 0.72$ AU (Venus orbital distance); panel (c) VEN3: VTGCM GJ 436 Venus at $d = 0.387$ AU (Mercury orbital distance); panel (d) VEN4: VTGCM GJ 436 Venus at $d = 0.175$ AU (closest orbital distance). All panels are at 2.5°N latitude, local time noon, and for pressures ranging from ~ 50 to 10^{-12} mbar. Kelvin (K)/day units are used throughout.

Venus at $d = 0.72$ AU (Venus orbital distance); panel (c, VEN4-1×) VTGCM GJ 436 Venus at $d = 0.175$ AU (closest orbital distance), VEN4 with the 1× NIR heating profile (Figure 7); and panel (d, VEN4-4×) VTGCM GJ 436 Venus at $d = 0.175$ AU, VEN4 with the 4× NIR heating profile (Figure 7).

Table 2 and Figure 9 show from our calculations that the dayside local noon geopotential height maximum progressively bulges with increasing NIR heating, ballooning from $\sim 300 \pm 20$ km for the VEN1, VEN2, and VEN3 cases (*cf.*, Table 2) out to 680 km for the VEN4-1.0× case and 760 km for the VEN4-4.0× case (*cf.*, Table 3). Typical nightside local midnight geopotential height maxima are ~ 210 km for the VEN1, VEN2, and VEN3 cases, yielding dayside noon to nightside midnight elongation ratios of $\sim 3:2$. Correspondingly, from Figure 9, it is seen that the nightside local midnight geopotential height maximum is ~ 220 and ~ 250 km for the VEN4 2.0× case and the VEN4 4.0× case, respectively, giving a remarkable approximate dayside noon to nightside midnight elongation ratio of $\sim 3:1$ for these cases.

Figure 10 represents the impact of the NIR heating variations on the climatological zonal wind. As was evident in Figure 3, the VTGCM simulations have much faster winds for all cases on the ET than on the MT, located at 18 and 6 hr, respectively. The maximum MT and ET wind speeds are tabulated in Table 3, and we see that the maxima for both the MT and ET wind speeds increased by 100–50 m/s, respectively, for our VEN4-4.0× case over the VEN4-1.0× case. This makes the ET winds remarkably fast at 650 m/s. The effect of quadrupling the NIR heating profile compared to doubling, Figure 7, shows the maximum wind speed increases are much greater for this case than

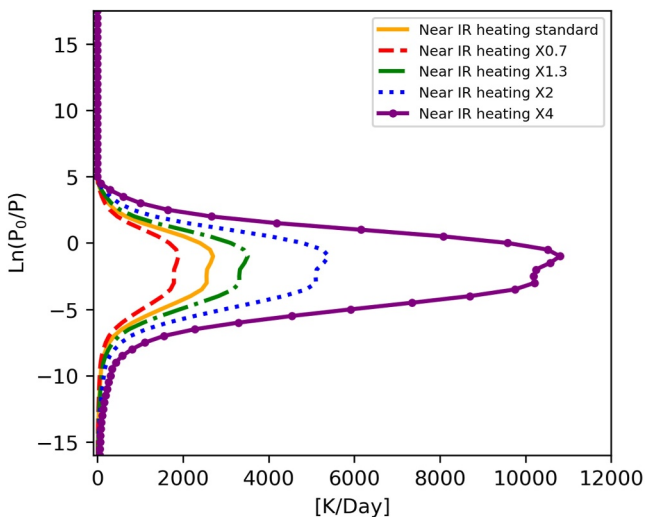


Figure 7. Changes to the standard reference NIR (std. ref. NIR) heating profile for the energy balance sensitivity study. Shown are 0.7× std. ref. NIR (“0.7×”, red dashed), standard reference NIR (“1×”, gold solid), 1.3× std. ref. NIR (“1.3×”, green dot dashed), 2.0× std. ref. NIR (“2×”, blue dotted), 4.0× std. ref. NIR (“4×”, purple solid with dots) heating profiles. Kelvin (K)/day units are used for pressures ranging from ~ 50 to 10^{-12} mbar.

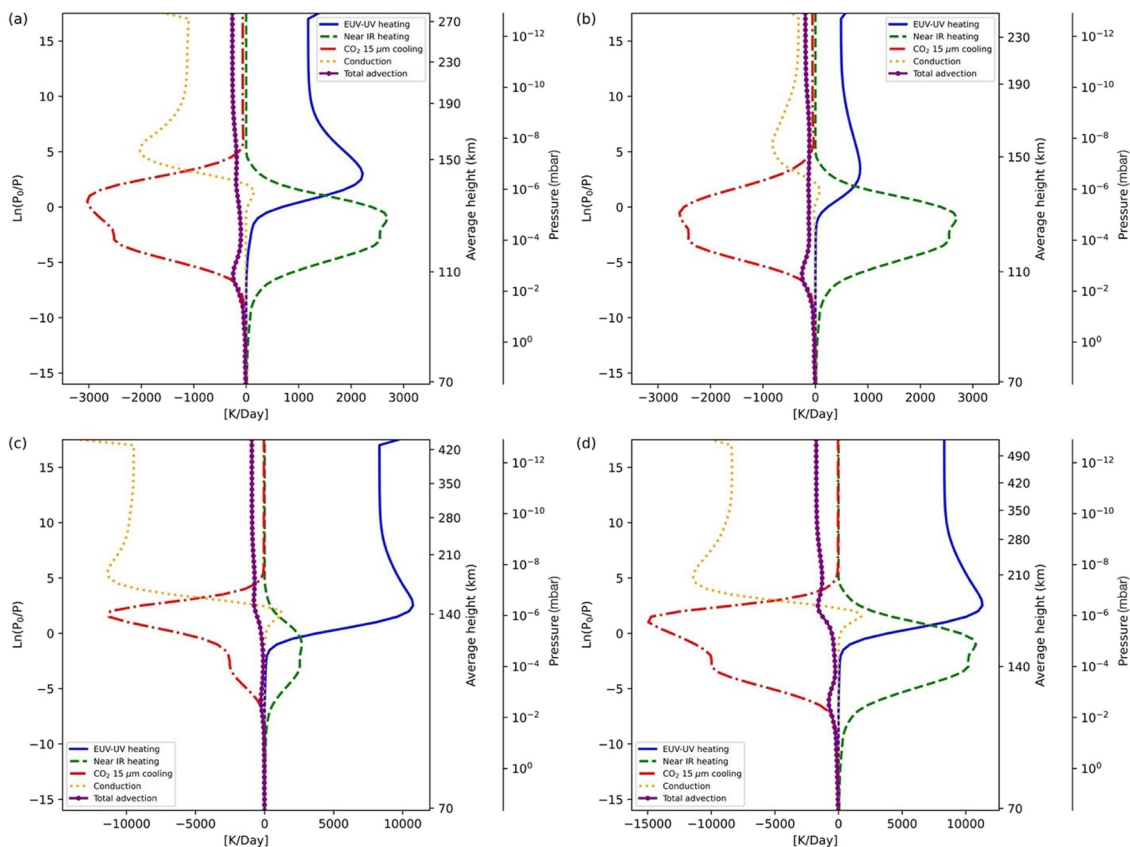


Figure 8. Energy balance sensitivity study analysis by varying the std. ref. NIR heating. Panel (a) **VEN1**: shows the present-day Venus Thermospheric General Circulation Model (VTGCM) baseline case for solar minimum conditions (validated against Venus Express observations); panel (b) **VEN2**: VTGCM GJ 436 Venus at $d = 0.72$ AU (Venus orbital distance); panel (c) **VEN4**: VTGCM GJ 436 Venus at $d = 0.175$ AU (closest orbital distance), VEN4 1× std. ref. heating profile shown in Figure 6; panel (d) **VEN4b**: VTGCM GJ 436 Venus at $d = 0.175$ AU, VEN4 4× std. ref. NIR heating profile shown in Figure 6. All panels are at 2.5°N latitude (equatorial) and Kelvin per day (K/day) units are used throughout. All panels are for pressures ranging from ~ 50 to 10^{-12} mbar.

those for changes occurring due to successive changes from $1.3\times$ and $2.0\times$ the standard reference NIR profile. The progressive increase in the top of the nightside midnight geopotential height and the dramatic increase in and distribution of the MT and ET zonal winds shown in Figures 9 and 10, panels (a)–(d), is further proof that nightside energy is provided by atmospheric circulation rather than radiation.

From our simulations, $0.7\times$ NIR cools and $1.3\times$ NIR warms dayside temperatures near the relative pressure given by $\ln(P_0/P)$ of -6.0 to -5.0 by about ± 10 K (not shown). Additionally, for the relative pressure region at pressures above $\ln(P_0/P) = -10$ in Figure 6, there was little or no change in the temperature structure and comparing Figure 6 panel (d) and Figure 11 panels (a) and (b), we see that this corresponds to a temperature of ~ 160 K for VEN1 and VEN2, respectively. However, we see in Figure 11 panel (d) for this region that there is a net 80 K increase in temperature to about 240 K for the VEN4-4× NIR case.

The greatest sensitivity to varying the NIR heating is higher up in the lower thermosphere and upper mesosphere as expected. For the region where $\ln(P_0/P) \geq 0$, $\pm 30\%$ changes in the NIR heating don't induce much change in nightside peak temperatures and the dayside peak temperatures warm (cool) by about only +15 K (-15 K) compared to the $1.0\times$ standard reference NIR heating profile case shown in Figure 6 panel (d). Thus, from our simulations, we see that these moderate changes in the NIR heating do not result in large changes in temperature over the standard reference NIR heating case. However, doubling and quadrupling the NIR heating profile produces significant changes in the entire temperature structure of the upper and middle atmosphere. Nightside peak temperatures increase by as much as 30 K and the dayside peak temperatures warm by a dramatic 50 and 130 K for the doubled and quadrupled NIR heating profiles compared to the $1.0\times$ standard reference NIR heating

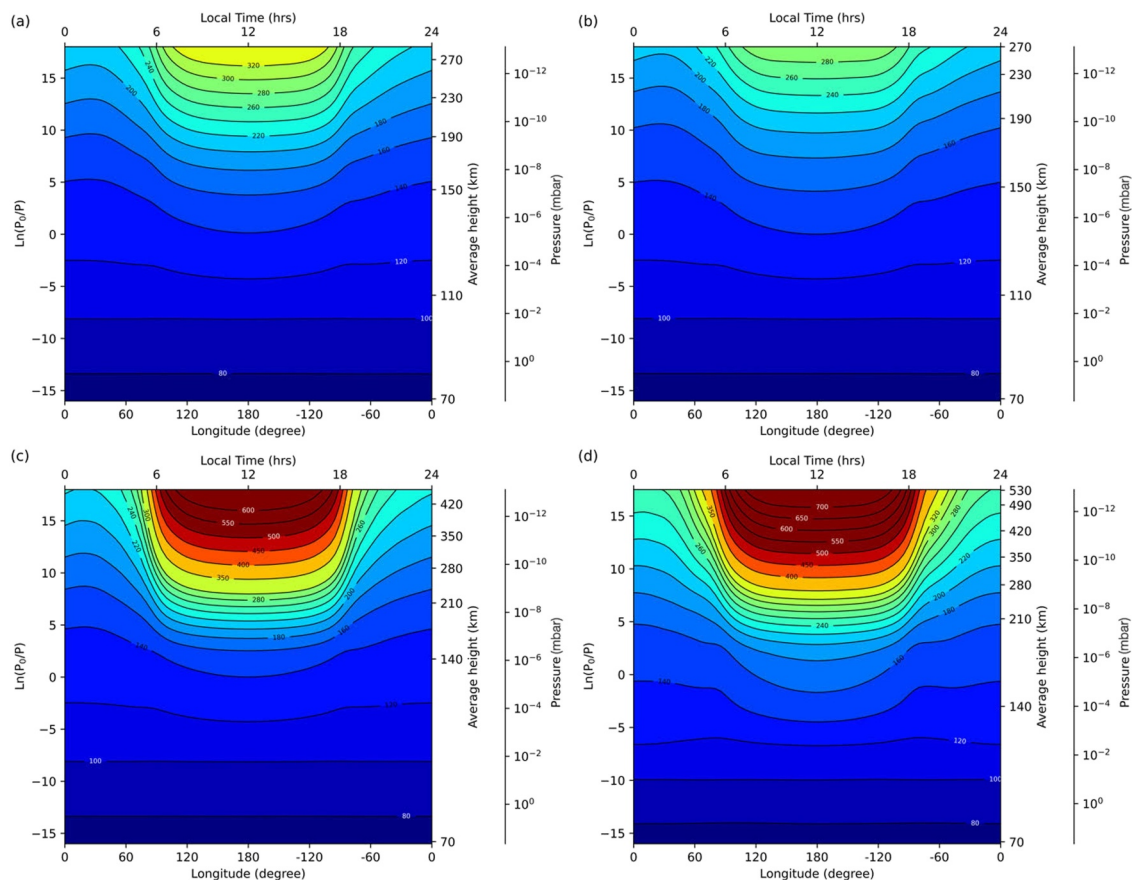


Figure 9. Geopotential Height results for the energy balance sensitivity study. Panel (a) **VEN1**: shows the present-day Venus Thermospheric General Circulation Model (VTGCM) baseline case for solar minimum conditions (validated against Venus Express observations); panel (b) **VEN2**: VTGCM GJ 436 Venus at $d = 0.72$ AU (Venus orbital distance); panel (c) **VEN4**: VTGCM GJ 436 Venus at $d = 0.175$ AU (closest orbital distance), VEN4 1× std. ref. heating profile shown in Figure 6; panel (d) **VEN4b**: VTGCM GJ 436 Venus at $d = 0.175$ AU, VEN4 4× std. ref. NIR heating profile shown in Figure 6. All panels are at 2.5°N latitude (equatorial) and for pressures ranging from ~ 50 to 10^{-12} mbar.

profile case shown in Figure 6 panel (d). At the $\ln(P_0/P) = 3\text{--}5$ level (just above the dT/dz inflection point) we have a doubling of absolute temperature between panels (b) and (d) in this region.

In the context of atmospheric escape studies, the Lambda parameter (Λ) is a dimensionless quantity that compares thermal energy and gravitational energy to characterize the relative gravitational influence on atmospheric particles. It is defined as the ratio of the gravitational energy to the thermal energy of atmospheric particles, given by the expression $\Lambda = (GMm_i/r)/kT$, with r being taken either as the distance from the center of the planet to the exobase or the location of the molecule(s) of mass, m_i , in question (Gronoff et al., 2020). A higher Λ value indicates that a planet's gravity retains its atmosphere more effectively, whereas a lower Λ suggests that atmospheric particles can escape more readily. It is to be noted that even an exospheric temperature in excess of 500 K, slightly less than twice the Venusian one, means that Λ (Gronoff et al., 2020) of atmospheric escape is about 11. This implies that we are far from hydrodynamic escape (it would require values below 2.5) and ensures a low atmospheric escape rate under quiet stellar conditions. The high Λ value results from the efficiency of CO_2 15- μm cooling (e.g., Bouger et al., 1986, 1988), which has significant implications for thermal escape in dense CO_2 -rich exoplanets. Most thermal escape studies to date have not considered CO_2 15- μm cooling as a mechanism for balancing the heat flux that drives escape. To the best of our knowledge, previous exoplanet studies have not accounted for this effect either, making it a novel and important consideration in the modeling of exoplanetary atmospheres.

Table 3 summarizes some key results of the sensitivity of changes in the NIR heating profile on the energy balance discussed above for our close-in dense CO_2 -rich exoplanetary atmosphere orbiting the M-dwarf star GJ 436.

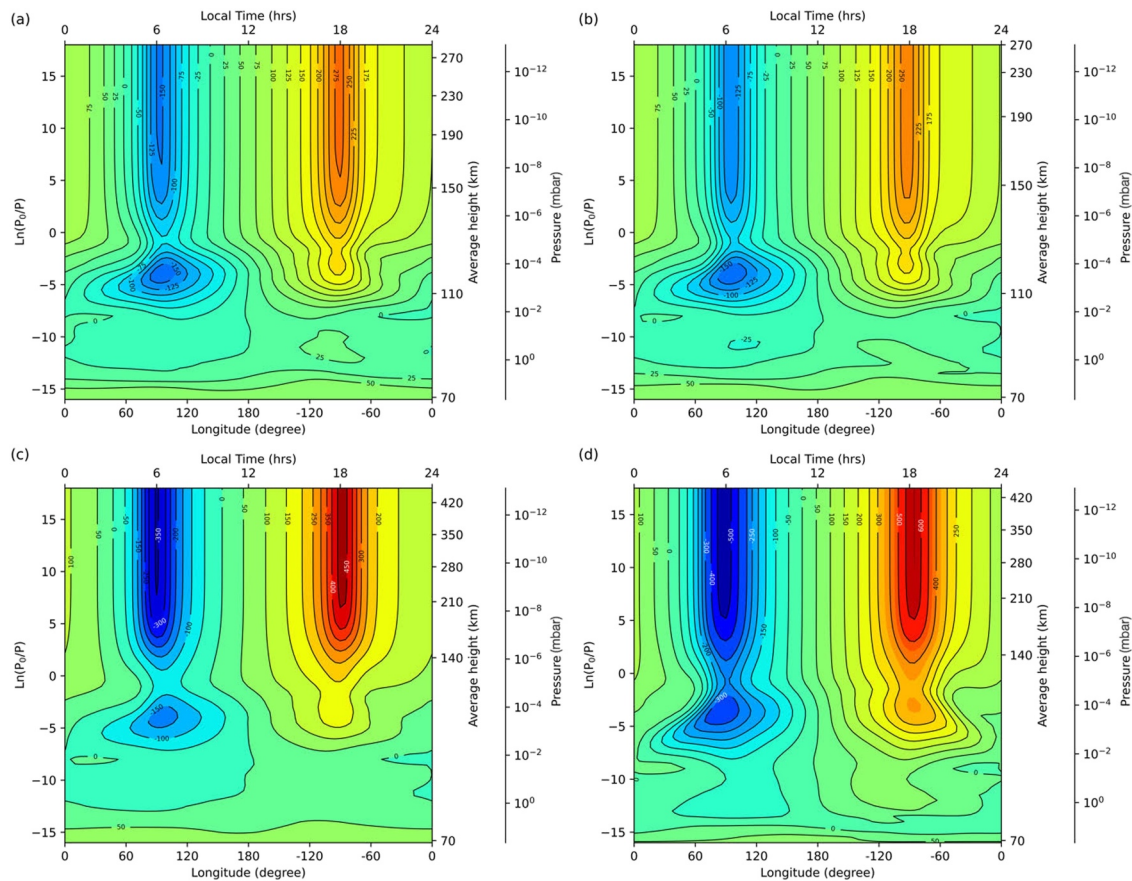


Figure 10. $u(z)$ Zonal Wind results for the energy balance sensitivity study. Panel (a) **VEN1:** shows the present-day Venus Thermospheric General Circulation Model (VTGCM) baseline case for solar minimum conditions (validated against Venus Express observations); panel (b) **VEN2:** VTGCM GJ 436 Venus at $d = 0.72$ AU (Venus orbital distance); panel (c) **VEN4:** VTGCM GJ 436 Venus at $d = 0.175$ AU (closest orbital distance), VEN4 1 \times std. ref. heating profile shown in Figure 6; panel (d) **VEN4b:** VTGCM GJ 436 Venus at $d = 0.175$ AU, VEN4 4 \times std. ref. NIR heating profile shown in Figure 6. All panels are at 2.5°N latitude (equatorial) and m/s units are used throughout. All panels are for pressures ranging from ~ 50 to 10^{-12} mbar. The sign convention is defined in Table 2 caption.

Remarkably, we see that even in the extreme cases shown, the enhanced non-LTE CO₂ 15-μm cooling still provides a strong thermostat that helps to regulate dayside temperatures for pressures of 10^{-7} to 10^{-2} mbar.

4. Conclusions

This study presents the first three dimensional simulations of a Venus-like exoplanet's upper atmosphere, integrating dynamics, energetics, and photochemistry to explore observable signatures under varying stellar irradiation. Key findings and implications include:

4.1. Thermal Regulation by CO₂ 15-μm Cooling

The CO₂ 15-μm cooling mechanism acts as a robust thermostat, maintaining stable dayside temperatures (pressures of 10^{-7} – 10^{-2} mbar) even under extreme EUV-UV and NIR heating. Without this cooling, dayside thermospheric temperatures would be significantly higher, as seen in our simulations of close-in orbits (e.g., 345 K warming at 0.175 AU). This process suppresses thermal escape, suggesting that dense CO₂-rich atmospheres around M-dwarfs may be more stable than previously assumed.

4.2. Dynamical Responses to Stellar Forcing

- Terminator Winds: ET winds dominate over MT winds due to Venus-like SS-AS circulation, with speeds exceeding 650 m/s under 4 \times NIR heating.

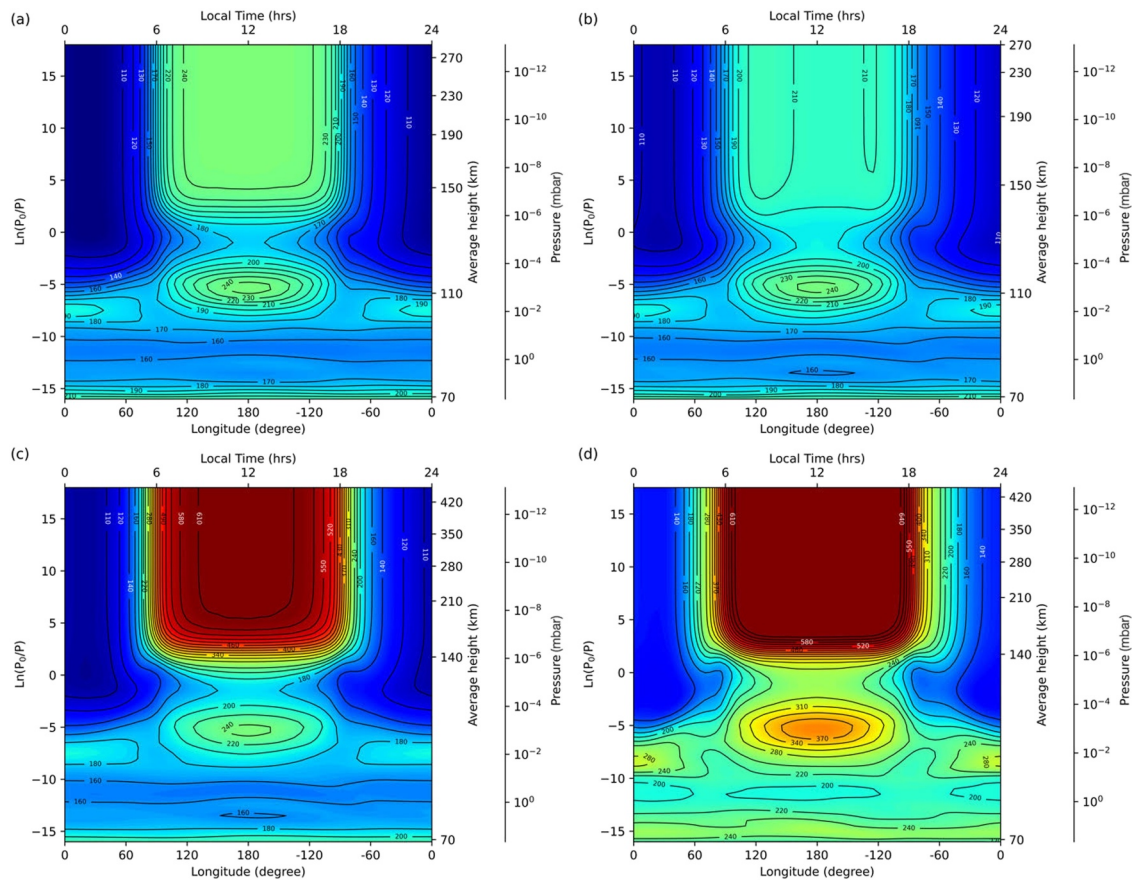


Figure 11. Neutral Temperature results for the energy balance sensitivity study. Panel (a) **VEN1**: shows the present-day Venus Thermospheric General Circulation Model (VTGCM) baseline case for solar minimum conditions (validated against Venus Express observations); panel (b) **VEN2**: VTGCM GJ 436 Venus at $d = 0.72$ AU (Venus orbital distance); panel (c) **VEN4**: VTGCM GJ 436 Venus at $d = 0.175$ AU (closest orbital distance), VEN4 1 \times std. ref. heating profile shown in Figure 6; panel (d) **VEN4b**: VTGCM GJ 436 Venus at $d = 0.175$ AU, VEN4 4 \times std. ref. NIR heating profile shown in Figure 6. All panels are at 2.5°N latitude (equatorial) and Kelvin (K) units are used throughout. All panels are for pressures ranging from ~ 50 to 10^{-12} mbar.

- Atmospheric Inflation: Dayside geopotential heights bulge to 760 km ($4\times$ NIR) versus nightside (~ 250 km), a 3:1 asymmetry driven by radiative forcing. Nightside temperatures remain stable, indicating energy redistribution via dynamics rather than direct heating.

4.3. Observational and Habitability Implications

- False Biosignatures: The combination of suppressed escape and high FUV/NUV ratios could lead to abiotic O_2/O_3 accumulation, posing challenges for life detection.

Table 3
Near Infrared Sensitivity Study: Various Parameters From Figures 8–11

Case	NIR multiplicative factor	Max geopotential height near equator (km) and noon:midnight atmospheric elongation ratio	Dayside T_{exo} noon near equator (K)	Max MT versus ET winds near equator (m/s)	Max dayside CO_2 15- μm cooling and EUV/UV/IR heat balance ^a (K/day)
VEN4	0.7	620 ($\sim 2.25:1$)	610	-300/ + 400	$\sim 10,920$
VEN4	1.3	640 ($\sim 2.25:1$)	640	-350/ + 450	$\sim 11,700$
VEN4a	2.0	680 ($\sim 3:1$)	670	-400/ + 500	$\sim 12,600$
VEN4b	4.0	760 ($\sim 3:1$)	750	-500/ + 650	$\sim 14,940$

Note. Sign convention is defined in Table 2 caption. ^aAll days are terrestrial days.

- Spectral Diagnostics: Strong CO₂ 15-μm emission peaks may distinguish Venus-like exoplanets via JWST or ELT observations, particularly for tidally locked targets.
- Habitable Zone Refinement: Our results suggest that atmospheric retention—not just HZ placement—should guide target prioritization, as CO₂ cooling extends the survivability of thick atmospheres even under high irradiation. This is consistent with previous work published by other authors discussing habitable zone placement (e.g., Kasting, 1995; Luger & Barnes, 2015; Meadows, 2017; Wordsworth & Pierrehumbert, 2014).

4.4. Limitations and Future Work

- The current model excludes wavelengths >250 nm, underestimating NUV-driven O₃ photolysis. Future updates will extend to 400 nm to capture catalytic cycles fully.
- Time-dependent flare effects and non-thermal escape processes warrant investigation to assess cumulative atmospheric loss.

This study provides a first benchmark and quantitative reference for the 3-D coupled photochemical–dynamical structure of a CO₂-rich terrestrial exoplanet around an M dwarf. While we do not present spectra, the detailed composition fields and vertical distributions form a critical link between climate simulations and spectral predictions, laying the foundation for interpreting future observations with JWST and beyond. This underscores the need for fully coupled GCM–photochemistry frameworks to robustly connect climate, chemistry, and observables.

Conflict of Interest

The authors declare no conflicts of interest relevant to this study.

Data Availability Statement

All data sets used for supporting the conclusions of this article are available from the University of Michigan Deep Blue Data Repository (see Bouger & Parkinson, 2022). Specifically, VTGCM data cubes are provided for eight separate simulation cases, capturing state variables and heat balance terms.

Acknowledgments

CDP would like to acknowledge Danica Adams who assisted with the plotting of the figures in this paper. CDP was supported in part by a NASA XRP grant number 80NSSC25K7166. YLY was supported in part by an NAI Virtual Planetary Laboratory grant from the University of Washington.

References

- Airapetian, V. S., Barnes, R., Cohen, O., Collinson, G. A., Danchi, W. C., Dong, C. F., et al. (2019). Impact of space weather on climate and habitability of terrestrial-type exoplanets. *International Journal of Astrobiology*, 19(2), 136–194. <https://doi.org/10.1017/s1473550419000132>
- Airapetian, V. S., Glocer, A., Gronoff, G., Hébrard, E., & Danchi, W. (2016). Prebiotic chemistry and atmospheric warming of early Earth by an active young Sun. *Nature Geoscience*, 9(6), 452–455. <https://doi.org/10.1038/ngeo2719>
- Arney, G., Domagal-Goldman, S. D., Meadows, V. S., Schwamb, E. W., Charnay, B., Claire, M., et al. (2016). The pale orange dot: The spectrum and habitability of hazy Archean Earth. *Astrobiology*, 16(11), 873–899. <https://doi.org/10.1089/ast.2015.1422>
- Arney, G. N. (2019). The K dwarf advantage for biosignatures on directly imaged exoplanets. *The Astrophysical Journal*, 837(1), L7. <https://doi.org/10.3847/2041-8213/ab0651>
- Arney, G. N., Meadows, V. S., Domagal-Goldman, S. D., Deming, D., Robinson, T., Tovar Mendoza, G., et al. (2017). Pale orange dots: The impact of organic haze on the habitability and detectability of Earthlike exoplanets. *The Astrophysical Journal*, 836(1), 49. <https://doi.org/10.3847/1538-4357/836/1/49>
- Bouger, S. W., Alexander, M. J., & Mayr, H. G. (1997). Upper atmosphere dynamics: Global circulation and gravity waves. *Venus II*, 2, 259–292.
- Bouger, S. W., Bell, J. M., Elrod, M. K., Mahaffy, P. R., Benna, M., Jakosky, B. M., & the MAVEN Team. (2015). Variability of Mars thermosphere neutral structure from MAVEN deep dip observations: NGIMS comparisons with global models. *AGU Fall Meeting Abstracts*, 2015, P21A–2064.
- Bouger, S. W., Brain, D. A., Fox, J. L., Gonzalez-Galindo, F., Simon-Wedlund, C., & Withers, P. G. (2017). Chapter 14: Upper Atmosphere and ionosphere. In B. Haberle, M. Smith, T. Clancy, F. Forget, & R. Zurek (Eds.), *The atmosphere and climate of Mars*. Cambridge University Press. <https://doi.org/10.1017/9781107016187>
- Bouger, S. W., Brecht, A. S., Schulte, R., Fischer, J.-L., Parkinson, C. D., Mahieux, A., et al. (2015). Upper atmosphere temperature structure at the Venusian terminators: A comparison of SOIR and VTGCM results. *Planetary and Space Science*, 113–114, 336–346. <https://doi.org/10.1016/j.pss.2015.01.012>
- Bouger, S. W., Dickinson, R. E., Ridley, E. C., & Roble, R. G. (1988). Venus mesosphere and thermosphere III. Three-dimensional general circulation with coupled dynamics and composition. *Icarus*, 73(3), 545–573. [https://doi.org/10.1016/0019-1035\(88\)90064-4](https://doi.org/10.1016/0019-1035(88)90064-4)
- Bouger, S. W., Engel, S., Roble, R. G., & Foster, B. (1999). Comparative terrestrial planet thermospheres: 2. Solar cycle variation of global structure and winds at equinox. *Journal of Geophysical Research*, 104(E7), 16591–16611. <https://doi.org/10.1029/1998je001019>
- Bouger, S. W., Hunten, D. M., & Phillips, R. J. (1986). Venus mesosphere and thermosphere: II. Global circulation, temperature, and density variations. *Icarus*, 68(2), 284–312. [https://doi.org/10.1016/0019-1035\(86\)90023-4](https://doi.org/10.1016/0019-1035(86)90023-4)
- Bouger, S. W., Jakosky, B. M., Halekas, J. S., Brain, D. A., MAVEN Science Team, Mahaffy, P., et al. (2015). Early MAVEN deep dip campaign reveals thermosphere and ionosphere variability. *Science*, 350(6261), aad0459. <https://doi.org/10.1126/science.aad0459>
- Bouger, S. W., & Parkinson, C. D. (2022). Venus-like exoplanet simulations: Temperature, wind and energy balance datasets using the VTGCM [Dataset]. *University of Michigan Deep Blue Data*. <https://doi.org/10.7302/VTAZ-TW05>

- Bougher, S. W., Pawlowski, D., Bell, J. M., Nelli, S., McDunn, T., Murphy, J. R., et al. (2015). Mars Global Ionosphere-Thermosphere Model (MGITM): Solar cycle, seasonal, and diurnal variations of the Mars upper atmosphere. *Journal of Geophysical Research: Planets*, 120(2), 311–342. <https://doi.org/10.1002/2014JE004715>
- Bougher, S. W., Rafkin, S., & Drossart, P. (2006). Dynamics of the Venus upper atmosphere: Outstanding problems and new constraints expected from Venus Express. *Planetary and Space Science*, 54(13–14), 1371–1380. <https://doi.org/10.1016/j.pss.2006.04.023>
- Bougher, S. W., Roble, R. G., & Fuller-Rowell, T. (2002). Simulations of the upper atmospheres of the terrestrial planets. *Geophysical Monograph Series*, 130, 261–288. <https://doi.org/10.1029/130gm17>
- Brecht, A. S. (2011). *Tracing the dynamics in Venus' upper atmosphere*, dissertation. University of Michigan.
- Brecht, A. S., & Bougher, S. W. (2012). Dayside thermal structure of Venus' upper atmosphere characterized by a global model. *Journal of Geophysical Research: Planets*, 117, E8. <https://doi.org/10.1029/2012JE004079>
- Brecht, A. S., Bougher, S. W., Gérard, J. C., Parkinson, C. D., Rafkin, S., & Foster, B. (2011). Understanding the variability of nightside temperatures, NO UV and O₂ IR nightglow emissions in the Venus upper atmosphere. *Journal of Geophysical Research*, 116(E8), E08004. <https://doi.org/10.1029/2010je003770>
- Brecht, A. S., Bougher, S. W., Gérard, J. C., & Soret, L. (2012). Atomic oxygen distributions in the Venus thermosphere: Comparisons between Venus Express observations and global model simulations. *Icarus*, 117, 759–766.
- Brecht, A. S., Bougher, S. W., Shields, D., Liu, H. L., & Lee, C. (2021). Planetary-Scale wave impacts on the venusian upper mesosphere and lower thermosphere. *Journal of Geophysical Research*, 126(1), e2020JE006587. <https://doi.org/10.1029/2020JE006587>
- Butler, R. P., Vogt, S. S., Marcy, G. W., Fischer, D. A., Wright, J. T., Henry, G. W., et al. (2004). A Neptune-mass planet orbiting the nearby M dwarf GJ 436. *The Astrophysical Journal*, 617(1), 580–588. <https://doi.org/10.1086/425173>
- Dickinson, R. E., & Ridley, E. C. (1977). Venus mesosphere and thermosphere temperature structure. II—Day-night variations. *Icarus*, 30(1), 163–178. [https://doi.org/10.1016/0019-1035\(77\)90130-0](https://doi.org/10.1016/0019-1035(77)90130-0)
- Domagal-Goldman, S. D., Segura, A., Claire, M. W., Robinson, T. D., & Meadows, V. S. (2014). Abiotic ozone and oxygen in atmospheres similar to prebiotic Earth. *The Astrophysical Journal*, 792(2), 90. <https://doi.org/10.1088/0004-637x/792/2/90>
- Ehrenreich, D., Bourrier, V., Wheatley, P. J., Lecavelier des Etangs, A., Huitson, C. M., Lavie, B., et al. (2015). A giant comet-like cloud of hydrogen escaping the warm Neptune-mass exoplanet GJ 436b. *Nature*, 522(7557), 459–461. <https://doi.org/10.1038/nature14501>
- Fauchez, T. J., Turbet, M., Villanueva, G. L., Schwertner, E. W., Arney, G. N., Robinson, T. D., et al. (2019). Impact of clouds and hazes on the simulated JWST transmission spectra of habitable zone planets in the TRAPPIST-1 system. *The Astrophysical Journal*, 887(2), 194. <https://doi.org/10.3847/1538-4357/ab5862>
- Fels, S. B. (1977). Momentum and energy exchanges due to orographically scattered gravity waves. *Journal of the Atmospheric Sciences*, 34(3), 499–514. [https://doi.org/10.1175/1520-0469\(1977\)034<499:maedt>2.0.co;2](https://doi.org/10.1175/1520-0469(1977)034<499:maedt>2.0.co;2)
- France, K., Froning, C. S., Linsky, J. L., Roberge, A., Stocke, J. T., Tian, F., et al. (2013). The ultraviolet radiation environment around M dwarf exoplanet host stars. *The Astrophysical Journal*, 763(2), 149. <https://doi.org/10.1088/0004-637x/763/2/149>
- Fujii, Y., Del Genio, A. D., & Amundsen, D. S. (2017). NIR-driven moist upper atmospheres of synchronously rotating temperate terrestrial exoplanets. *The Astrophysical Journal*, 848(2), 100. <https://doi.org/10.3847/1538-4357/aa8955>
- Gao, P., Hu, R., Robinson, T. D., Li, C., & Yung, Y. L. (2015). Stability of CO₂ atmospheres on desiccated M dwarf exoplanets. *The Astrophysical Journal*, 806(2), 249. <https://doi.org/10.1088/0004-637X/806/2/249>
- Gilli, G., López-Valverde, M. A., Peralta, J., Bougher, S., Brecht, A., Drossart, P., & Piccioni, G. (2015). Carbon monoxide and temperature in the upper atmosphere of Venus from VIRTIS/Venus Express non-LTE limb measurements. *Icarus*, 248, 478–498. <https://doi.org/10.1016/j.icarus.2014.10.047>
- Grenfell, J. L., Gebauer, S., Godolt, M., Palczynski, K., Rauer, H., Stock, J., et al. (2013). Potential biosignatures in super-Earth atmospheres II. Photochemical responses. *Astrobiology*, 13(5), 415–438. <https://doi.org/10.1089/ast.2012.0926>
- Gronoff, G., Arras, P., Baraka, S., Bell, J. M., Bonfond, B., Brandt, P. C., et al. (2020). Atmospheric escape processes and planetary atmospheric evolution. *Journal of Geophysical Research: Space Physics*, 125(8), e2019JA027639. <https://doi.org/10.1029/2019JA027639>
- Harman, C. E., Felton, F., Hu, R., Domagal-Goldman, S. D., Segura, A., Tian, F., & Kasting, J. F. (2018). Abiotic O₂ levels on planets around F, G, K, and M stars: Effects of lightning-produced catalysts in eliminating oxygen false positives. *The Astrophysical Journal*, 866(1), 56. <https://doi.org/10.3847/1538-4357/aad9b>
- Harman, C. E., Schwertner, E. W., Schottelkotte, J. C., & Kasting, J. F. (2015). Abiotic O₂ levels on planets around F, G, K, and M stars: Possible false positives for life? *The Astrophysical Journal*, 812, 137. <https://doi.org/10.1088/0004-627X/812/2/137>
- Hu, R., Peterson, L., & Wolf, E. T. (2020). O₂-dominated atmospheres for potentially habitable environments on TRAPPIST-1 planets. *The Astrophysical Journal*, 888(2), 122. <https://doi.org/10.3847/1538-4357/ab5ffc>
- Kane, S. R., Arney, G., Crisp, D., Domagal-Goldman, S., Glaze, L., Goldblatt, C., et al. (2019). Venus as a laboratory for exoplanetary science. *Journal of Geophysical Research: Planets*, 124(8), 2015–2028. <https://doi.org/10.1029/2019je005939>
- Kane, S. R., Arney, G., Graham, H. V., Hoffman, J., Ramirez, R. M., Robinson, T. D., & Zahnle, K. (2021). Venus and the degeneracy of habitability. *Journal of Geophysical Research: Planets*, 126(6), e2021JE006643. <https://doi.org/10.1029/2021JE006643>
- Kane, S. R., Ceja, A. Y., Way, M. J., & Quintana, E. V. (2018). Climate modeling of a potential ExoVenus. *The Astrophysical Journal*, 869(1), 46. <https://doi.org/10.3847/1538-4357/aaec68>
- Kane, S. R., Kopparapu, R. K., & Domagal-Goldman, S. D. (2014). On the frequency of potential Venus analogs from Kepler data. *The Astrophysical Journal*, 794(1), L5. <https://doi.org/10.1088/2041-8205/794/1/L5>
- Kasting, J. (1995). O₂ concentrations in dense primitive atmospheres: Commentary. *Planetary and Space Science*, 43(1–2), 11–13. [https://doi.org/10.1016/0032-0633\(94\)00203-4](https://doi.org/10.1016/0032-0633(94)00203-4)
- Kowalski, A. F., Hawley, S. L., Hilton, E. J., Becker, A. C., West, A. A., Bochanski, J. J., & Sesar, B. (2009). M dwarfs in Sloan Digital Sky Survey Stripe 82: Photometric light curves and flare rate analysis. *The Astronomical Journal*, 138(2), 633–648. <https://doi.org/10.1088/0004-6256/138/2/633>
- Ledvina, S. A., & Brecht, S. H. (2020). Features of the Venus solar wind interaction due to the orbital motion of Venus. In *AGU fall meeting abstracts* (Vol. 2020, p. P046-0010).
- Lee, C., Lawson, W. G., Richardson, M. I., Anderson, J. L., Collins, N., Hoar, T., & Mischna, M. (2011). Demonstration of ensemble data assimilation for Mars using DART, MarsWRF, and radiance observations from MGS TES. *Journal of Geophysical Research*, 116(E11), E11011. <https://doi.org/10.1029/2011je003815>
- Lee, C., & Richardson, M. I. (2010). A general circulation model ensemble study of the atmospheric circulation of Venus. *Journal of Geophysical Research*, 115(E4), E04002. <https://doi.org/10.1029/2009je003490>

- Lellouch, E., Clancy, T., Crisp, D., Kliore, A. J., Titov, D., & Bouger, S. W. (1997). Monitoring of mesospheric structure and dynamics. In S. W. Bouger, D. M. Hunten, & R. J. Phillips (Eds.), *Venus II: Geology, geophysics, atmosphere, and solar wind environment* (pp. 295–324). Univ. of Ariz. Press.
- Lincowski, A. P., Meadows, V. S., Crisp, D., Robinson, T. D., Luger, R., Lustig-Yaeger, J., & Arney, G. N. (2018). Evolved climates and observational discriminants for the TRAPPIST-1 planetary System. *The Astrophysical Journal*, 867, 1–34. <https://doi.org/10.3847/1538-4357/aae36a>
- Loyd, R. P., Schneider, P. C., Jackman, J. A., France, K., Shkolnik, E. L., Arulanantham, N., et al. (2024). Erratum: “Flares, Rotation, Activity Cycles, and a Magnetic Star–Planet Interaction Hypothesis for the Far-ultraviolet Emission of GJ 436” (2023, AJ, 165, 146). *The Astronomical Journal*, 167(4), 185. <https://doi.org/10.3847/1538-3881/ad2de0>
- Luger, R., & Barnes, R. (2015). Extreme Water Loss and Abiotic O₂ buildup on planets throughout the habitable zones of M Dwarfs. *Astrobiology*, 15, 2–143. <https://doi.org/10.1089/ast.2014.1231>
- Mayne, N. J., Baraffe, I., Boulte, I. A., Acreman, D. M., Smith, C., Browning, M. K., et al. (2014). The unified model and the simulation of hot Jupiters. *Astronomy & Astrophysics*, 561, A1. <https://doi.org/10.1051/0004-6361/201322174>
- Meadows, V. S. (2017). Reflections on O₂ as a biosignature in exoplanetary atmospheres. *Astrobiology*, 17(10), 1022–1052. <https://doi.org/10.1089/ast.2016.1578>
- Meadows, V. S., Arney, G. N., Schwertner, E. W., Lustig-Yaeger, J., Lincowski, A. P., Robinson, T., et al. (2018). The habitability of Proxima Centauri b: Environmental States and observational discriminants. *Astrobiology*, 18(2), 133–189. <https://doi.org/10.1089/ast.2016.1589>
- Mendonça, J. M., Grimm, S. L., Grosheintz, L., & Heng, K. (2016). THOR: A new and flexible global circulation model to explore planetary atmospheres. *The Astrophysical Journal*, 829(2), 115. <https://doi.org/10.3847/0004-637X/829/2/115>
- Mickol, R. L., Farris, H. N., Kohler, E., Chevrier, V., Kral, T. A., & Lacy, C. (2015). A simple one-dimensional radiative-convective atmosphere model for use with extrasolar atmospheres. In *46th Lunar and Planetary Science Conference (abstract #1255)*. Lunar and Planetary Institute.
- Mills, F. P., Moses, J. I., Gao, P., & Tsai, S.-M. (2021). The diversity of planetary atmospheric chemistry: Lessons and challenges from our solar system and extrasolar planets. *Space Science Reviews*, 217(3), 43. <https://doi.org/10.1007/s11214-021-00810-1>
- National Research Council. (2000). *One universe: At home in the cosmos*. The National Academies Press. <https://doi.org/10.17226/9585>
- Parkinson, C. D., Bouger, S. W., Brecht, A. S., Gao, P. S., & Yung, Y. L. (2018). On understanding the nature and variation of the Venusian middle atmosphere via observations and numerical modeling of key tracer species. In *Venera-D Venus modeling workshop* (pp. 59–62). Space Research Institute (IKI).
- Parkinson, C. D., Brecht, A., Bouger, S., Mills, F., Yung, Y. L., Shields, D., & Liemohn, M. (2021). Modeling of observations of the OH nightglow in the venusian mesosphere. *Icarus*, 368, 114580. <https://doi.org/10.1016/j.icarus.2021.114580>
- Parkinson, C. D., Gao, P. S., Schulte, R., Bouger, S. W., Yung, Y. L., Bardeen, C. G., et al. (2015). Distribution of sulphuric acid aerosols in the clouds and upper haze of Venus using Venus Express VAST and VeRa temperature profiles. *Planetary and Space Science*, 113–114, 205–218. <https://doi.org/10.1016/j.pss.2015.01.023>
- Parkinson, C. D., Yung, Y., Esposito, L., Gao, P., Bouger, S. W., & Hirtzig, M. (2015). Photochemical control of the distribution of venusian water and comparison to Venus Express SOIR observations. *Planetary and Space Science*, 113–114, 226–236. <https://doi.org/10.1016/j.pss.2015.02.015>
- Pawlowski, D. J., & Ridley, A. J. (2008). Modeling the thermospheric response to solar flares. *Journal of Geophysical Research: Space Physics*, 113(A10), A10309. <https://doi.org/10.1029/2008JA013182>
- Pawlowski, D. J., & Ridley, A. J. (2009a). Modeling the ionospheric response to the 28 October 2003 solar flare due to coupling with the thermosphere. *Radio Science*, 44(1), RS0A23. <https://doi.org/10.1029/2008RS004081>
- Pawlowski, D. J., & Ridley, A. J. (2009b). Quantifying the effect of thermospheric parameterization in a global model. *Journal of Atmospheric and Solar-Terrestrial Physics*, 71(17–18), 2017–2026. <https://doi.org/10.1016/j.jastp.2009.09.007>
- Pidhorodetska, D., Pidhorodetska, D., Fauchez, T. J., Villanueva, G. L., Domagal-Goldman, S. D., & Kopparapu, R. K. (2020). Detection of neutral magnesium escaping the atmosphere of a hot Jupiter. *The Astrophysical Journal*, 898(2), L33. <https://doi.org/10.3847/2041-8213/aba4a1>
- Robinson, T. D., & Catling, D. C. (2012). An analytic radiative-convective model for planetary atmospheres. *The Astrophysical Journal*, 757(1), 104. <https://doi.org/10.1088/0004-637x/757/1/104>
- Robinson, T. D., & Crisp, D. (2018). Linearized Flux Evolution (LiFE): A technique for rapidly adapting fluxes from full-physics radiative transfer models. *Journal of Quantitative Spectroscopy & Radiative Transfer*, 211, 78–95. <https://doi.org/10.1016/j.jqsrt.2018.03.002>
- Rypdal, M. (2017). *Astrophysics II lecture notes*. Department of Physics, Norwegian University of Science and Technology (NTNU). Retrieved from https://web.phys.ntnu.no/~mika/skript_astroIup3.pdf
- Schubert, G., Bouger, S. W., Covey, A. D., Del Genio, C. C., Grossman, A. S., Hollingsworth, J. L., et al. (2007). Venus atmosphere dynamics: A continuing enigma. In L. W. Esposito, E. R. Stofan, & T. E. Cravens (Eds.), *Exploring Venus as terrestrial planet, geophysics monograph series* (Vol. 176, pp. 121–138). AGU. <https://doi.org/10.1029/176gm07>
- Schubert, G., Covey, C., Genio, A. D., Elson, L. S., Keating, G., Seiff, A., et al. (1980). Structure and circulation of the Venus atmosphere. *Journal of Geophysical Research*, 85(A13), 8007–8025. <https://doi.org/10.1029/JA085iA13p08007>
- Segura, A., Kasting, J. F., Meadows, V., Cohen, M., Scalo, J., Crisp, D., et al. (2005). Biosignatures from Earth-like planets around M dwarfs. *Astrobiology*, 5(6), 706–725. <https://doi.org/10.1089/ast.2005.5.706>
- Segura, A., Krelove, K., Kasting, J. F., Sommerlatt, D., Meadows, V., Crisp, D., et al. (2003). Ozone concentrations and ultraviolet fluxes on Earth-like planets around other stars. *Astrobiology*, 3(4), 689–708. <https://doi.org/10.1089/153110703322736024>
- Segura, A., Meadows, V. S., Kasting, J. F., Crisp, D., & Cohen, M. (2007). Abiotic formation of O₂ and O₃ in high-CO₂ terrestrial atmospheres. *Astronomy & Astrophysics*, 472, 665.
- Segura, A., Walkowicz, L., Meadows, V., Kasting, J., & Hawley, S. (2010). The effect of a strong stellar flare on the atmospheric chemistry of an earth-like planet orbiting an M dwarf. *Astrobiology*, 10(7), 751–771. <https://doi.org/10.1089/ast.2009.0376>
- Showman, A. P., Wordsworth, R. D., Merlis, T. M., & Kaspi, Y. (2013). Atmospheric circulation of terrestrial exoplanets. In S. Seager (Ed.), *Exoplanets* (pp. 277–326). University of Arizona Press.
- Terrien, R. C., Mahadevan, S., Deshpande, R., & Bender, C. F. (2015). A technique for determining M dwarf metallicities using K-band spectra. *The Astrophysical Journal Supplement Series*, 220(1), 16. <https://doi.org/10.1088/0067-0049/220/1/16>
- Tian, F., France, K., Linsky, J. L., Mauas, P. J. D., & Vieytes, M. C. (2014). High stellar FUV/NUV ratio and oxygen contents in the atmospheres of potentially habitable planets. *Earth and Planetary Science Letters*, 385, 22–27. <https://doi.org/10.1016/j.epsl.2013.10.024>
- Tilley, M. A., Segura, A., Meadows, V. S., Hawley, S., & Davenport, J. (2019). Modeling repeated M dwarf flaring at an Earth-like planet in the habitable zone: Atmospheric effects for an unmagnetized planet. *Astrobiology*, 19(1), 64–86. <https://doi.org/10.1089/ast.2017.1794>

- Torres, G., Winn, J. N., & Holman, M. J. (2008). Improved parameters for extrasolar transiting planets. *The Astrophysical Journal*, 677(2), 1324–1333. <https://doi.org/10.1086/529429>
- Turbet, M., Bolmont, E., Chaveroche, G., Ehrenreich, D., Gillmann, C., Tosi, N., & Forget, F. (2021). Day-night cloud asymmetry prevents early oceans on Venus but not on Earth. *Nature*, 598(7880), 276–280. <https://doi.org/10.1038/s41586-021-03873-w>
- Turbet, M., Bolmont, E., Leconte, J., Forget, F., Selsis, F., Tobie, G., et al. (2018). Modeling climate diversity, tidal dynamics and the fate of volatiles on TRAPPIST-1 planets. *Astronomy & Astrophysics*, 612, A86. <https://doi.org/10.1051/0004-6361/201731620>
- Valeille, A., Combi, M. R., Tenishev, V., Bougner, S. W., & Nagy, A. F. (2009). A study of suprathermal oxygen atoms in Mars upper thermosphere and exosphere over the range of limiting conditions. *Icarus*, 206(1), 18–27. <https://doi.org/10.1016/j.icarus.2008.08.018>
- Valeille, A., Combi, M. R., Tenishev, V., Bougner, S. W., & Nagy, A. F. (2010). Three-dimensional study of Mars upper thermosphere/ionosphere and hot oxygen corona. *Journal of Geophysical Research: Planets*, 114, E11006. <https://doi.org/10.1029/2009JE003389>
- von Braun, K., Boyajian, T. S., Kane, S. R., Hebb, L., van Belle, G. T., Farrington, C. D., et al. (2012). The GJ 436 System: Directly determined astrophysical parameters of an M dwarf and implications for the transiting hot Neptune. *The Astrophysical Journal*, 753(2), 171. <https://doi.org/10.1088/0004-637X/753/2/171>
- Way, M. J., & Del Genio, A. D. (2020). Venusian habitable climate scenarios: Modeling Venus through time and applications to slowly rotating Venus-like exoplanets. *Journal of Geophysical Research: Planets*, 125(5), e2019JE006276. <https://doi.org/10.1029/2019JE006276>
- Way, M. J., Del Genio, A. D., & Amundsen, D. S. (2023). Exoplanetary atmospheres and the search for habitable worlds. *Space Science*, 219(13). <https://doi.org/10.1007/s11214-023-00962-1>
- Way, M. J., Del Genio, A. D., Kiang, N. Y., Sohl, L. E., Grinspoon, D. H., Aleinov, I., et al. (2016). Was Venus the first habitable world of our solar system? *Geophysical Research Letters*, 43(16), 8376–8383. <https://doi.org/10.1002/2016GL069790>
- Way, M. J., Del Genio, A. D., Kiang, N. Y., Sohl, L. E., Grinspoon, D. H., Aleinov, I., et al. (2017). Resolving orbital and climate keys of Earth and extraterrestrial environments with dynamics (ROCKE-3D). *The Astrophysical Journal Supplement Series*, 231(1), 12. <https://doi.org/10.3847/1538-4365/aa7a06>
- WMO. (1985). Atmospheric Ozone 1985. In *Assessment of our understanding of the processes controlling its present distribution and change, volume 1: Global ozone research and monitoring Project-Report No. 16*.
- Wolf, E. T. (2017). Assessing the habitability of Earth-like planets using the general circulation model ExoCAM. *The Astrophysical Journal*, 839(2), L1. <https://doi.org/10.3847/2041-8213/aa693a>
- Wordsworth, R., & Pierrehumbert, R. (2014). Abiotic oxygen-dominated atmospheres on terrestrial habitable zone planets. *The Astrophysical Journal Letters*, 785(2), L20. <https://doi.org/10.1088/2041-8205/785/2/L20>
- Wordsworth, R. D., Forget, F., Selsis, F., Millour, E., Charnay, B., & Madeléine, J.-B. (2011). Gliese 581d is the first discovered terrestrial-mass exoplanet in the habitable zone. *The Astrophysical Journal Letters*, 733(2), L48. <https://doi.org/10.1088/2041-8205/733/2/L48>
- Zhang, X., Liang, M.-C., Mills, F. P., Belyaev, D. A., & Yung, Y. L. (2012). Sulfur chemistry in the middle atmosphere of Venus. *Icarus*, 217(2), 714–739. <https://doi.org/10.1016/j.icarus.2011.06.016>
- Zhang, X., Liang, M.-C., Montmessin, F., Bertaux, J.-L., Parkinson, C., & Yung, Y. L. (2010). Photolysis of sulfuric acid as the source of sulfur oxides in the mesosphere of Venus. *Nature Geoscience*, 3(12), 834–837. <https://doi.org/10.1038/NGEO989>